

NASA Contractor Report 4691

User's Manual for the One-Dimensional Hypersonic Experimental Aero-Thermodynamic (1DHEAT) Data Reduction Code

Brian R. Hollis
North Carolina State University • Raleigh, North Carolina

National Aeronautics and Space Administration
Langley Research Center • Hampton, Virginia 23681-0001

Prepared for Langley Research Center
under Grants NAG1-1663 and NAGW-1331

August 1995

Printed copies available from the following:

NASA Center for AeroSpace Information
800 Elkridge Landing Road
Linthicum Heights, MD 21090-2934
(301) 621-0390

National Technical Information Service (NTIS)
5285 Port Royal Road
Springfield, VA 22161-2171
(703) 487-4650

TABLE OF CONTENTS

ACKNOWLEDGMENTS v

ABSTRACT 1

INTRODUCTION 1

SYMBOLS 2

ONE-DIMENSIONAL HEAT TRANSFER 3

TEST-TIME AND THE SEMI-INFINITE ASSUMPTION 4

HEAT TRANSFER MODELS 5

Constant thermal properties 5

Variable thermal conductivity 6

Variable thermal conductivity and thermal diffusivity 7

Finite-volume 7

1DHEAT CODE DESCRIPTION 8

OVERVIEW 8

INSTALLATION AND SETUP 8

NAMING CONVENTION AND DIRECTORY TREE 9

FILE DESCRIPTIONS 9

Input files 9

Output files 10

Error log 11

UNITS 11

HEAT TRANSFER COMPUTATIONS 12

STATISTICS 13

DATA REDUCTION AND ANALYSIS 14

FINITE-VOLUME APPLICATIONS 19

CONCLUDING REMARKS 20

REFERENCES 22

APPENDIX A. ANALYTICAL HEAT TRANSFER MODELS 24

APPENDIX B. FINITE-VOLUME HEAT TRANSFER MODEL 30

APPENDIX C. MATERIAL THERMAL PROPERTIES 34

MATERIAL PROPERTY CURVE FITS 34

Type-E Thermocouple 34

Chromel 35

Constantan....35
Macor....35
Quartz....36
Pyrex....37
17-4 Stainless Steel....37
CORRECTION FACTORS....38
ADDITIONAL MATERIALS....40
VALIDATION OF THERMAL PROPERTIES DATA....40
APPENDIX D. 1DHEAT INPUT FILES....42
SETUP FILE "1Ddemocoax.inp"....42
Listing of sample setup file "1Ddemocoax.inp"....42
Description of "1Ddemocoax.inp" file....42
FINITE-VOLUME SETUP FILE "1Ddemocoax.fvinp"....44
Listing of sample setup file "1Ddemocoax.fvinp"....44
Description of "1Ddemocoax.fvinp" file....44
INPUT TEMPERATURE FILE "1Ddemocoax.degk"....45
Listing of sample input file "1Ddemocoax.degk"....45
Description of "1Ddemocoax.degk" file....45

ACKNOWLEDGMENTS

This research was supported by grants NAGW-1331 and NAG-1-1663 to the North Carolina State University Mars Mission Research Center.

ABSTRACT

A FORTRAN computer code for the reduction and analysis of experimental heat transfer data has been developed. This code can be utilized to determine heat transfer rates from surface temperature measurements made using either thin-film resistance gages or coaxial surface thermocouples. Both an analytical and a numerical finite-volume heat transfer model are implemented in this code. The analytical solution is based on a one-dimensional, semi-infinite wall thickness model with the approximation of constant substrate thermal properties, which is empirically corrected for the effects of variable thermal properties. The finite-volume solution is based on a one-dimensional, implicit discretization. The finite-volume model directly incorporates the effects of variable substrate thermal properties and does not require the semi-infinite wall thickness approximation used in the analytical model. This model also includes the option of a multiple-layer substrate. Fast, accurate results can be obtained using either method. This code has been used to reduce several sets of aerodynamic heating data, of which samples are included in this report.

INTRODUCTION

Information on aerodynamic heating rates is a critical factor in the design of hypersonic vehicles. A common experimental technique for the determination of aerodynamic heat transfer rates is wind tunnel testing of models which have been instrumented with surface temperature sensors such as thin-film resistance gages or coaxial surface thermocouples. These sensors are used to measure surface temperatures during a wind-tunnel test, and the surface heat transfer rates are then calculated from the recorded time histories of the surface temperatures.

An analytical relationship between the heat transfer rate and the measured surface temperature-time history was developed by Vidal (ref. 1), and Schultz and Jones (ref. 2). This relationship is based on the model of one-dimensional heat transfer to a semi-infinite substrate which has constant thermal properties. Cook (ref. 3) extended this theory to include substrate materials with variable thermal conductivity. Hartunian and Varwig (ref. 4) and Miller (ref. 5) developed approximate correction factors to account for substrate materials with variable thermal conductivity and thermal diffusivity. The one-dimensional heat transfer problem with variable thermal properties has also been solved numerically by many authors, for example White (ref. 6), Patankar (ref. 7) and Dunn et al (ref. 8). Pittman and Brinkley (ref. 9) and Bradley and Throckmorton (ref. 10) have extended the numerical method to multiple-layer substrate problems.

In this report, the **One-D**imensional **H**ypersonic **E**xperimental **A**ero-**T**hermodynamic data reduction code, 1DHEAT, will be detailed. 1DHEAT is an fast, user-friendly FORTRAN code for heat transfer data reduction which incorporates both analytical and numerical models. Variable thermal properties are accounted for in both models, and

both models can be used to reduce either thin-film gage data or coaxial thermocouple data. Additionally, multiple-layer substrates can be dealt with using the finite-volume model.

SYMBOLS

C_h	Stanton number (dimensionless heat transfer coefficient), $\dot{q} / [\rho u_\infty (h_{aw} - h_\infty)]$
c_p	specific heat (J/kg-°K)
E	sensor voltage (mV or V)
h	enthalpy (J/kg)
H	dimensional heat transfer coefficient $\dot{q} / (h_{aw} - h_\infty)$
k	thermal conductivity (W/m-°K)
L()	Laplace transform of ()
$\dot{q}$	heat transfer rate (W/m^2)
Q	heat addition (J/m^2)
R	sensor resistance (Ω)
r	adiabatic wall recovery factor
RMS()	root-mean square of ()
S()	standard deviation of ()
s	Laplace transform variable
T	temperature (°K)
t	time (sec)
u	velocity (m/s)
x	depth through substrate(m)
x^*	dimensionless penetration depth
α	thermal diffusivity, $k / (\rho c_p)$ (m^2/s)
α_R	coefficient of resistance (1/°R)
β	thermal product, $\sqrt{\rho c_p k}$ (W-s$^{1/2}$/m^2-°K)
β'	correction factor
ϕ	transformed temperature, $\phi = \int_0^\theta \frac{k}{k_0} d\theta$ (°K)
λ	dummy time integration variable (s)
σ	mesh Fourier number, $\sigma = \frac{\alpha_0 \Delta t}{(\Delta x)^2}$

θ	temperature defined by $\theta(x,t) = T(x,t) - T(x,0)$ (°K)
ρ	density (kg/m^3)

SUBSCRIPTS

∞	freestream
0	initial (pre-test) condition
1	start of averaging window
2	end of averaging window
amb	ambient (pre-test)
cal	calibration condition
gage	surface temperature measured by gage
int	cell interface
l	left boundary
r	right boundary
rp	reference point temperature
ref	reference condition
s	surface temperature
tot	stagnation

ONE-DIMENSIONAL HEAT TRANSFER

Figure 1 depicts a generic surface temperature sensor mounted on a substrate material. For a thin-film gage, the sensor is typically a platinum or palladium film, and the substrate is a thermally insulative material such as Macor or quartz. For a coaxial thermocouple, the sensing element is a thin junction of two thermocouple materials, such as chromel and constantan, while the substrate is the body of the thermocouple. In either case, the sensor is typically designed so that the thickness of the sensing element is much less than that of the substrate. The sensing element, therefore, has a negligible effect on the heat transfer to the substrate, and the temperature measured by the sensing element is identical to the temperature at the surface of the substrate. It is also assumed that there is no lateral conduction through the substrate and that heat is conducted only in the direction normal to the surface. The final assumptions are that the substrate is of infinite depth, and that the temperature rise at infinity is zero. Together, these assumptions are referred to as the one-dimensional, semi-infinite solid model. Using this model, the temperature distribution in the substrate can be given by the partial differential equation

$$\frac{\partial}{\partial x}\left(k\frac{dT}{dx}\right)=\rho c_p\frac{\partial T}{\partial t} \tag{1a}$$

The thermal properties (thermal conductivity, specific heat and density) are all functions of temperature. The boundary conditions are given by

$$\begin{aligned} &T(x,t=t_0)=T_0\\ &T(x=0,t)=T_s(t)\\ &\dot{q}(x=\infty,t)=0 \end{aligned} \tag{1b}$$

A common simplification is the assumption of constant thermal properties, in which case the temperature distribution is given by

$$\frac{\partial^2 T}{\partial x^2}=\frac{1}{\alpha_0}\frac{\partial T}{\partial t}$$

where

$$\alpha_0=\frac{k}{\rho c_p}=\text{constant} \tag{2}$$

The boundary conditions are the same as for equation (1).

TEST-TIME AND THE SEMI-INFINITE ASSUMPTION

The semi-infinite substrate assumption, which is required for an analytical (but not numerical) solution of equation (1), is only approximately correct during an actual experiment. The accuracy of the assumption is a function of material depth, diffusivity and test duration, and can be measured in terms of the increase in the temperature or heat transfer rate at the back of the substrate. The relevant dimensionless parameter for the thermal penetration depth is given in reference 2

$$x^*=\frac{x}{2\sqrt{\alpha t}} \tag{3}$$

Expressions for the back face heat transfer and temperature for a constant heating rate were also derived in reference 2.

$$\frac{T_x}{T_s}=e^{(-x^*)^2}-\left(x^*\sqrt{\pi}\right)erfc(x^*) \tag{4a}$$

$$\frac{\dot{q}_x}{\dot{q}_s} = erfc(x^*) \tag{4b}$$

The period of the semi-infinite test time can be estimated from Figure 2 (which is redrawn from reference 2) as a function of the thickness of the substrate. Ideally, the substrate should be thick enough that the ratio $\dot{q}_x/\dot{q}_s$ at the back face of the substrate be no more than a few percent for the test time desired. Because the penetration depth is inversely proportional to the square root of diffusivity, materials with lower diffusivity (such as ceramics) have a longer semi-infinite test time, whereas high diffusivity materials (such as metals) have a shorter test time.

HEAT TRANSFER MODELS

Equation (1) can be solved to determine the temperature distribution, and thus the heat flux, either analytically or numerically (through the use of the finite-volume technique). Analytical solutions are possible for materials in which the thermal properties are constant or in which only the thermal conductivity varies with temperature; an empirical variable properties correction to the constant properties solution is also possible. Variable thermal properties are treated directly in the finite-volume solution method. These methods are summarized in this section, and are discussed in detail in Appendices A and B

Constant thermal properties

The simplest analytical solution (ref. 2) is found by assuming that the material properties are all independent of temperature. The surface heat flux can then be found from the measured time history of the surface temperature by

$$\dot{q}(t_n) = \dot{q}_n = \frac{2\beta_0}{\sqrt{\pi}} \sum_{i=1}^{i=n} \frac{T_i - T_{i-1}}{\sqrt{t_n - t_i} + \sqrt{t_n - t_{i-1}}} \tag{5}$$

where the thermal product

$$\beta_0 = \sqrt{\rho c_p k} \tag{6}$$

is evaluated at the ambient temperature. The derivation of equation (5) is presented in Appendix A.

Alternatively, the total heat added to the substrate can first be calculated using the method given by Kendall and Dixon (ref. 11)

$$Q_n = \frac{\beta_0}{\sqrt{\pi}} \sum_{i=1}^{i=n} \frac{T_i + T_{i-1}}{\sqrt{t_n - t_i} + \sqrt{t_n - t_{i-1}}} \Delta t \tag{7a}$$

and the heat transfer rate can then be computed with the finite-difference approximation used by Hedlund et al (ref. 12)

$$\dot{q}(t_n) = \dot{q}_n = \frac{dQ_n}{dt} = \frac{-2Q_{n-8} - Q_{n-4} + Q_{n+4} + 2Q_{n+8}}{40\Delta t} \tag{7b}$$

The schemes represented by equations (5) and (7) are referred to as the direct method and the indirect method, respectively. In general, the instantaneous heat transfer rates computed using the two methods are not identical. This is because the temperature difference term in the numerator of equation (5) of the direct method tends to accentuate fluctuations in $\dot{q}$, whereas the temperature sum term in the numerator of equation (7a) and the wide differencing stencil in equation (7b) of the indirect method tend to smooth fluctuations in $\dot{q}$. However, over a given time interval the average values of the heat flux will be approximately equal. The indirect method then, would be preferable in a situation where the random noise level is relatively high in comparison to the heat transfer rate. If however, the fluctuations in $\dot{q}$ were of interest, as for example in a turbulent flow, then the direct method would be preferable. Further discussion and comparisons between these two methods are presented in the Data Reduction and Analysis section.

Variable thermal conductivity

Equations (5) and (7) are based on the assumption of constant substrate thermal properties. In hypersonic heat transfer experiments, the increase in the temperature of the substrate is usually not negligible. This assumption then is not valid, and the above formulations are valuable only as starting points for more detailed analyses.

A more accurate analytical solution can be found by assuming that the thermal conductivity of the substrate is a function of temperature but that the thermal diffusivity is a constant (ref. 3).

$$\alpha = \frac{k}{\rho c_\rho} = \text{constant} \tag{8}$$

This is a reasonable approximation for metallic substrates, such as that of a coaxial thermocouple. With this assumption, the equations for the direct and indirect methods become

Direct method:

$$\dot{q}(t_n) = \frac{2\beta_0}{\sqrt{\pi}} \sum_{i=1}^{i=n} \frac{\phi_i - \phi_{i-1}}{\sqrt{t_n - t_i} + \sqrt{t_n - t_{i-1}}} \tag{9}$$

Indirect method:

$$Q_n = \frac{\beta_0}{\sqrt{\pi}} \sum_{i=1}^{i=n} \frac{\phi_i + \phi_{i-1}}{\sqrt{t_n - t_i} + \sqrt{t_n - t_{i-1}}} \Delta t \tag{10a}$$

$$\dot{q}(t_n) = \dot{q}_n = \frac{dQ_n}{dt} = \frac{-2Q_{n-8} - Q_{n-4} + Q_{n+4} + 2Q_{n+8}}{40\Delta t} \tag{10b}$$

where

$$\phi = \int_{T_0}^{T} \frac{k}{k_0} dT \tag{11}$$

Variable thermal conductivity and thermal diffusivity

Equations (9) and (10) are inadequate for the insulative substrates typically used with thin-film gages, such as Macor, quartz, or Pyrex. For these substrates, both the thermal conductivity and thermal diffusivity are functions of temperature. For this case, there are no exact closed form solutions for heat transfer such as given by equations (5,7) or (9,10). However, an accurate approximation for the heat transfer rate may be made through the use of a correction factor for the variation of material properties with temperature. This approach was first used by Hartunian and Varwig (ref. 4) for quartz and Pyrex substrates. Correction factors were also derived for Pyrex by Cook (refs. 13,14) and for Macor by Miller (ref. 5). New correction factors have been derived for Macor and quartz by comparison with finite-volume solutions, as detailed in Appendix C. The formulation for heat transfer with variable material properties is

$$\dot{q}_{\beta(T)} = \dot{q}_{\beta_0} [1 + \beta' \Delta T_s] \tag{12a}$$

where

$$\Delta T_s = T_{gage} - T_{amb} \tag{12b}$$

where β' is the correction factor which accounts for the variation of material properties and $\dot{q}_{\beta_0}$ is the constant material properties heat transfer rate computed using either the direct (eq. 5) or indirect method (eq. 7).

Finite-volume

When all thermal properties are functions of temperature, an "exact" solution to equation (1) can only be obtained through a finite-volume model of the substrate.

$$T_i^n = T(x_i, t^n) \tag{13}$$

The numerical model is more flexible than the analytical model in that the semi-infinite assumption does not need to be made; this assumption is replaced with a physical boundary condition at the interior (back-face) of the substrate. The boundary condition may be that of an adiabatic (zero heat transfer) back face, a constant temperature back-face, or a temperature measurement made using a second sensor located at the back face of the substrate. This finite wall thickness analysis is most useful because it is not uncommon for a wind tunnel model to have a wall thickness small enough that the semi-infinite assumption is violated during a test, which would result in incorrect heating rates being computed from a semi-infinite analysis. The finite-volume analysis also makes it possible to model a multiple-layer substrate. The finite-volume method is detailed in Appendix B.

1DHEAT CODE DESCRIPTION

OVERVIEW

The analytical and computational models discussed in the previous section have been incorporated into 1DHEAT. 1DHEAT is a flexible, user-friendly FORTRAN code for the reduction and analysis of experimental heat transfer data from thin-film and coaxial thermocouple surface temperature sensors. 1DHEAT has been compiled and executed on SUN and Hewlett-Packard workstations. Execution time is dependent on the number of temperature sensors, length of the data acquisition window, and the heat transfer data reduction model employed, but is typically on the order of a minute. As an example, a test with data from 70 thin-film gages with 4 seconds of data taken at a 50 Hz sampling rate (14000 data points) has been reduced in under 30 seconds on both Hewlett-Packard and SUN workstations

INSTALLATION AND SETUP

The 1DHEAT code and sample data sets are distributed in a tar file , '1DFILES', which is accompanied by an installation script file, '1DINST'. To install the 1DHEAT code, copy the files '1DFILES' and '1DINST' to the host computer and run the installation utility by typing "1DINST". The '1DINST' utility creates a home directory '1DHEAT' for 1DHEAT and installs the source code there. It also creates subdirectories for the sample data sets and installs the necessary raw data files and input files therein. The source code '1DHEAT.f' may then be compiled and immediately be used to reduce and analyze the sample data sets, as will be discussed in the section "Data Reduction

and Analysis". To reduce new data sets, raw data input files and setup files must first be created, as will be detailed in the next sections.

NAMING CONVENTION AND DIRECTORY TREE

The 1DHEAT code uses or creates several files for each data set which is analyzed. In order to avoid confusion, 1DHEAT data files' names follow a specific naming convention, and are organized in an hierarchical directory tree based on wind tunnel test series and run number identifiers. The 1DHEAT directory tree is depicted in Figure 3. The naming convention for 1DHEAT data files is '1D**testIDrunID**.*ext*', where '**testID**' and '**runID**' are the identifiers for the test series and run number identifier of a data set. These identifiers may each be any combination of up to six numerals and/or characters (upper or lower case). The extension '*ext*' denotes the file types, which are summarized in Table 1. A file name example is '1DT293R005.*ext*', which would designate the 5th run in test series 293.

For each test series, the user must create a subdirectory 'test**testID**' under the parent directory in which the 1DHEAT source code resides. For each run in a test series, the user must create a subdirectory 'run**runID**' in the 'test**testID**' subdirectory. All input files for a given run must be placed in that run subdirectory; 1DHEAT automatically places the output files in the appropriate run subdirectories.

FILE DESCRIPTIONS

Input files

'1D**testIDrunID**.inp'

'1D**testIDrunID**.fvinp'

'1D**testIDrunID**.degk'

'1D**testIDrunID**.volt'

To reduce experimental data with the 1DHEAT code, a setup file and a raw data file for each data set which is to be analyzed must be provided by the user; if the finite-volume model is to be used in the data reduction, an additional finite-volume setup file is also required.

The setup file, '1D**testIDrunID**.inp', contains entries on flow properties, gage and substrate types and other information which is required for the reduction of the raw data. The finite-volume setup file, '1D**testIDrunID**.fvinp' contains information on the number of substrate layers, the thickness of each layer, and the number of computational nodes to be used for each layer. Examples of each of these file types are given in Appendix D along with descriptions of the entries in the files.

The raw input data for 1DHEAT may be either the sensor output voltage-time histories or the temperature-time histories computed by the user from the voltage-temperature calibrations of the sensors. The raw data files for these options are entitled '1D**testIDrunID**.volt' and '1D**testIDrunID**.degk', respectively. If raw voltages are to be input, the voltage-temperature calibrations must be of the same form as those in the 1DHEAT code. For thin-film gages, the voltage-temperature relationship used is based on the calibration methods used at the Langley Research Center:

$$T = T_{amb} + \frac{\Delta E}{E_{amb}\alpha_R}[1 + \alpha_R(T_{amb} - T_{cal})] \tag{14}$$

where subscript 'cal' refers to calibration conditions, subscript 'amb' refers to ambient pre-test conditions and ΔE is the measured gage output (relative to pre-test baseline) in millivolts. For coaxial gages the conversion is the NBS standard for Type-E (chromel-constantan) thermocouples

$$T = T_{rp} + \sum_{i=0}^{i=9} a_i E^i \tag{15}$$

where E is the absolute measured gage output (which must be in volts for the NBS curve fit) and T_{rp} is the reference point temperature of 273 °K (freezing point of water). The coefficients of equation (21) are listed in Table 2. If gages with different voltage-temperature calibrations than these are utilized, the user must first convert the voltage-time history to a temperature-time history.

Output files

'1D**testIDrunID**.t'

'1D**testIDrunID**.qx'

'1D**testIDrunID**.chx'

'1D**testIDrunID**.distx'

'1D**testIDrunID**.distxnew'

'1D**testIDrunID**.qresx'

'1D**testIDrunID**.chresx'

'1D**testIDrunID**.tback'

'1D**testIDrunID**.*gageid*'

Several output files are created for the results computed using each of the data reduction methods. The method is identified by the number '*x*' in the file extension, which corresponds to computations based on:

x=1) Indirect Analytical Method:

Equation (7) with the correction in (12) for thin film gages, or equation (10) for coaxial thermocouples.

x=2) Direct Analytical Method:

Equation (5) with the correction in (12) for thin film gages, or equation (9) for coaxial thermocouples.

x=3) Finite-Volume Method:

Numerical solution of equation (13) for either gage type.

The output files '1D**testIDrunID**.qx' and '1D**testIDrunID**.chx' contain the time histories for each gage of the heat transfer rate and the Stanton number, respectively. The '1D**testIDrunID**.distx' file contains the averaged surface distributions of the heat transfer rate, q, Stanton number, C_h, the dimensional heat transfer coefficient, H, and the extrapolated reference temperature heating rate, q_{ref}, as well as the standard deviations of the averaged heat transfer rate and Stanton number and their root-mean square values. The surface heating distributions are all based on the time-averaging window specified in the input file. The user may recompute these values based on a different averaging window, in which case the new distributions are written to the '1D**testIDrunID**.distxnew' file. The output files '1D**testIDrunID**.qresx' and '1D**testIDrunID**.chresx' contain the time histories of the heat transfer rate residual and Stanton number residual, respectively. Finally, the '1D**testIDrunID**.t' file contains the temperature-time history for each gage. The quantities above are all defined in the Heat Transfer Computations section.

The '1D**testIDrunID**.tback' and '1D**testIDrunID**.*gageid*' files are unique to the finite-volume method. The '1D**testIDrunID**.tback' file contains the temperature-time history of the back face node of each gage, and can be used to estimate the validity of the semi-infinite assumption. The '1D**testIDrunID**.*gageid*' file contains the temperature profile through the substrate of sensor "*gageid*" at a user-specified time.

Error log

The 1DHEAT code generates an error log entitled '1DHEAT.errorlog' which resides in the 1DHEAT root directory. This file contains a record of any errors which occurred during a session and is automatically output to the screen at the end of the session. The error log can be useful in identifying problems with the setup or data files, and as a record of any errors which occur if 1DHEAT is run in batch mode.

UNITS

All input data used by 1DHEAT must be in SI units except for the thin-film gage coefficient of resistance, α_R, (in the '1D**testIDrunID**.inp' file) which has units of (1/°R) (to agree with the current format for gage calibration data at NASA LaRC) and the gage surface position data (also in the '1D**testIDrunID**.inp' file) which may be in any system of units. No computations are made with the position data; it is only included to allow the

user to plot surface heating distributions. All output data is in SI units with the exception of the gage position data in the '1D**testIDrunID**.distx' and '1D**testIDrunID**.distxnew' files.

HEAT TRANSFER COMPUTATIONS

The 1DHEAT code computes the time histories of the heat transfer rate for each gage using the method specified by the user. After the heat transfer rates have been computed, the dimensional heat transfer coefficient, H, and the dimensionless heat transfer coefficient (Stanton number), C_h, can be computed by

$$H = \frac{\dot{q}}{(\Delta h_{aw} - \Delta h_w)} \tag{16}$$

and

$$C_h = \frac{\dot{q}}{\rho_\infty u_\infty (\Delta h_{aw} - \Delta h_w)} \tag{17}$$

where the enthalpies are defined by:

$$\Delta h_w = h(T_w) - h(T_{rp}) \tag{18a}$$

$$\Delta h_{aw} = h(T_{aw}) - h(T_{rp}) \tag{18b}$$

The factor $h(T_{rp})$ is the enthalpy at a user-defined reference point temperature. The enthalpies in equations (18a) and (18b) are written as differences to remind the user that the computations for the wall and adiabatic wall enthalpies MUST be based on the same reference point temperature. For perfect gas flows, the reference point enthalpy is usually taken as zero at 0° K, while for chemically reacting flows it is sometimes taken to be zero at the standard temperature of 298°K. The reference point in 1DHEAT is 298°K.

The adiabatic wall enthalpy is related to the total enthalpy by

$$\Delta h_{aw} = \Delta h_0 + (r-1)\frac{u_\infty^2}{2} \tag{19}$$

and the recovery factor, r, is 1 for a stagnation point and for a flat plate is typically taken as $Pr^{1/2}$ for laminar flow or $Pr^{1/3}$ for turbulent flow. Note that in equation (19) it is assumed that the edge velocity is equal to the freestream velocity, and thus the Stanton number computations in 1DHEAT are based on freestream as opposed to boundary

layer edge conditions. This approximation is made in order to simplify the setup file formats and reduce the amount of data that the user must provide.

A "reference" heating rate can also be computed. This is an estimate of the value of the heat flux at a specified wall temperature (such as the ambient temperature), and should not be confused with the reference temperature, T^* of boundary layer computations. Assuming that the heat transfer coefficient for a particular gage remains constant with time (allowing for experimental noise and measurement error), the reference heat transfer rate can be extrapolated from an averaged Stanton number by:

$$\dot{q}_{ref} = \overline{C}_h \cdot \left[\rho_\infty u_\infty \left(\Delta h_{aw} - \Delta h_{ref}\right)\right] \tag{20}$$

The recovery factor, reference temperature, freestream velocity and total enthalpy are all user inputs in the setup file, while the wall enthalpies are computed in 1DHEAT from the temperature-time histories of the sensors.

STATISTICS

After the heat transfer computations are made, 1DHEAT performs a statistical analysis of the heat transfer data by computing the RMS (root mean squares) values and the standard deviations of the averaged heat transfer rate and Stanton number. The RMS values are given by

$$RMS(\dot{q}) = \sqrt{\frac{1}{n_{avg}} \sum_{n=i_1}^{n=i_1+n_{avg}} \left(\dot{q}_n\right)^2} \tag{21}$$

and the standard deviations are given by

$$S(\dot{q}) = \sqrt{\frac{\sum_{n=i_1}^{n=i_1+n_{avg}} \left(\dot{q}_n\right)^2 - n_{avg}\left(\overline{\dot{q}}\right)^2}{n_{avg} - 1}} \tag{22}$$

The formulas for the Stanton number values have the same form. In equations (21-22), i_1 and $(i_1 + n_{avg})$ are the time indices of the start and end of the averaging window.

The standard deviation is indicative of the experimental uncertainty of the time-averaged values, which can be influenced by factors such as flow quality and gage electrical noise. If the data is free from electrical noise produced either by the sensor or the data acquisition system, and the flow quality is high (and laminar) and the heat transfer rate (or Stanton number) is constant, then the standard deviation should tend toward zero. Data from

individual sensors which show significantly higher standard deviations than other nearby sensors should be considered suspect as this suggests poor sensor performance. Overall higher standard deviations may suggest either system-wide electrical noise or significant freestream unsteadiness or turbulence.

The normalized time history of the residual of the heating rates has been found to a useful parameter with which to characterize the wake flow-establishment process in short-duration (test times of milliseconds or less) test facilities (Hollis and Perkins, ref. 15). The normalized residual is given by

$$\Delta\hat{\dot{q}}_i = \frac{\left(\frac{\partial \dot{q}}{\partial t}\right)_i \Delta t}{\dot{q}_i} \tag{23a}$$

or for the Stanton number by

$$\left(\Delta\hat{C}_h\right)_i = \frac{\left(\frac{\partial C_h}{\partial t}\right)_i \Delta t}{\left(C_h\right)_i} \tag{23b}$$

The derivatives in equation (23) are numerically approximated by a four-point central derivative of the same form as equation (10b) for the indirect method, and by two-point central derivatives for the direct and finite-volume methods. The establishment process over the entire body is characterized by an RMS of the heat transfer rates of all the sensors (with a similar form for the Stanton number):

$$RMS(\Delta\dot{q})_i = \left[\frac{1}{ngages}\left(\Delta\dot{q}^{(1)} + \Delta\dot{q}^{(2)} + \ldots + \Delta\dot{q}^{(ngages)}\right)\right]^{\frac{1}{2}} \tag{24}$$

Because the residual values are dependent on the heat transfer model and the numerical derivative approximation, they should be considered a qualitative, not quantitative source of data. Also note that this RMS computation is spatial (based on data from gages at different positions at a given time) as opposed to the temporal computation (based on data from the same gage at different times) of equation (21).

DATA REDUCTION AND ANALYSIS

The data reduction and analysis options available in 1DHEAT are listed in the 1DHEAT main menu, which is shown in Figure 4. The options are divided into two groups: semi-infinite options and finite-volume options.

Options 1 and 2 correspond to the semi-infinite solution methods of equations (5) and (7) with the correction for variable thermal properties of equation (12) for thin-film gages, and to equations (9) and (10) for coaxial thermocouples. Options 5 and 6 correspond to the finite-volume numerical method of equation (13). The

output from any of the above options consists of files containing the temperature-time histories ('1D**testIDrunID**.t'), the heating rate-time histories ('1D**testIDrunID**.qx'), and the Stanton number-time histories of each gage ('1D**testIDrunID**.chx'). Additionally, the averages and statistics for the heating computations over the specified time window are output to ('1D**testIDrunID**.distx'). Options 3 or 7 are used to recompute these averages over a new time-averaging window (output to '1D**testIDrunID**.distxnew'). Options 4 or 8 are used to output the residual time histories of the heat rate and Stanton number. Finally, option 9 is used to compute the temperature distribution (using the finite-volume method) through the substrate of a single gage at a specified time (output to '1D**testIDrunID**.*gageid*').

These options can be explored using the sample data sets created by the installation utility. The sample data is identified by the test series "demo"; in this test series are two runs: "coax" and "thin" (the file name templates for these data are thus 1Ddemocoax.*ext* and 1Ddemothin.*ext*, respectively). The "democoax" data set is from a run in the NASA Langley Research Center 31" Mach 10 Air Tunnel (this facility is described by Micol in ref. 16) of a 2" radius hemisphere instrumented with Type-E coaxial surface thermocouples. The "demothin" data set is from a run in the same facility of a 70° sphere-cone (0.5" nose radius, 0.05" corner radius, and 2" base diameter) with thin-film gages on a Macor substrate.

A 1DHEAT session is illustrated on the following pages using the "democoax" data as an example. 1DHEAT output is shown in bold face and user keyboard input in shown in italics.

First, the raw data from the "democoax" set is reduced using the semi-infinite methods (direct and indirect):

```
          "1DHEAT" v2.20 PROGRAM OPTIONS:

     SEMI-INFINITE METHOD
          1.  Reduce raw data (volts).
          2.  Reduce raw data (degrees K).
          3.  Recompute statistics over new
              time interval.
          4.  Compute residuals.

     FINITE-VOLUME METHOD
          5.  Reduce raw data (volts).
          6.  Reduce raw data (degrees K).
          7.  Recompute statistics over new
              time interval.
          8.  Compute residuals.
          9.  Temperature profile for a gage at a
              specified time.

          10. Quit.
```

```
Enter your choice. (1-10) 2
Enter test ID (up to six characters) demo
Enter run ID (up to six characters) coax

Opened setup file: testdemo/runcoax/1Ddemocoax.inp

Opened temperature data file: testdemo/runcoax/1Ddemocoax.degk
Reading data for    7 gages
```

```
Read   501 data points per gage for    7 gages

Computing dQ/dt  ( 351 points per gage)...
Integration window:    1.72       (sec) to    8.32       (sec)
Finished computing dQ/dt

Computing q  ( 351 points per gage)...
Integration window:    1.72       (sec) to    8.32       (sec)
Finished computing q

Computing statistics for     7 gages
Averaging window:    4.00       (sec) to    5.00       (sec)

Writing data...
Finished writing data for
Test:  demo
Run:  coax
```

After examination of the reduced data to determine a more exact data-averaging window, 1DHEAT is used to re-average the data over a new time interval:

```
"1DHEAT" v2.20 PROGRAM OPTIONS:

    SEMI-INFINITE METHOD
         1.  Reduce raw data (volts).
         2.  Reduce raw data (degrees K).
         3.  Recompute statistics over new
             time interval.
         4.  Compute residuals.

    FINITE-VOLUME METHOD
         5.  Reduce raw data (volts).
         6.  Reduce raw data (degrees K).
         7.  Recompute statistics over new
             time interval.
         8.  Compute residuals.
         9.  Temperature profile for a gage at a
             specified time.

         10. Quit.
```

```
Enter your choice. (1-10) 3
Enter test ID (up to six characters) demo
Enter run ID (up to six characters) coax

Opened setup file:  testdemo/runcoax/1Ddemocoax.inp
Opened reduced data file:  testdemo/runcoax/1Ddemocoax.q1
Opened reduced data file:  testdemo/runcoax/1Ddemocoax.q2
Opened reduced data file:  testdemo/runcoax/1Ddemocoax.ch1
Opened reduced data file:  testdemo/runcoax/1Ddemocoax.ch2

Reduced data runs from    1.72       (sec)
                     to   8.32       (sec)

Enter start time (sec) of averaging window. 3.75
```

```
Enter end time (sec) of averaging window. 4.25

Computing statistics for     7 gages
Averaging window:    3.75       (sec) to    4.25       (sec)

Writing data
Finished writing data for
Test: demo
Run: coax
```

Additional data sets can now be reduced, or as in this example, the program can be exited.

```
-------------------------------------------------
|            "1DHEAT" v2.20 PROGRAM OPTIONS:    |
|                                               |
|     SEMI-INFINITE METHOD                      |
|          1. Reduce raw data (volts).          |
|          2. Reduce raw data (degrees K).      |
|          3. Recompute statistics over new     |
|             time interval.                    |
|          4. Compute residuals.                |
|                                               |
|     FINITE-VOLUME METHOD                      |
|          5. Reduce raw data (volts).          |
|          6. Reduce raw data (degrees K).      |
|          7. Recompute statistics over new     |
|             time interval.                    |
|          8. Compute residuals.                |
|          9. Temperature profile for a gage at a |
|             specified time.                   |
|                                               |
|          10. Quit.                            |
-------------------------------------------------

Enter your choice. (1-10) 10
SESSION ENDS
```

The reduced data from this session and from reduction of the "demothin" data set are useful in illustrating the features of the 1DHEAT code. Data from the "democoax" set is plotted in Figures 5 through 9. Data from the "demothin" set is plotted in Figures 10 through 17. Flow conditions for these two runs are given in Table 3.

The measured temperature-time histories of the thermocouples on the hemisphere (seven, distributed along a single ray at 15° increments) from the "democoax" data set are plotted in Figure 5. This data is found in the '1Ddemocoax.t' file. Note that because of the high diffusivity and conductivity of the thermocouples, the temperature rise, and thus the increase in wall enthalpy, was small during the test. Because the wall enthalpy increase was small the heat transfer rate (which is proportional to the difference between the flow stagnation enthalpy and the wall enthalpy) remained nearly constant through the duration of the run.

The time histories of the heat flux at the stagnation point gage ($\theta = 0$) as computed using both the direct and the indirect method are shown in Figure 6. These time histories are found in the '1Ddemocoax.q1' and

'1Ddemocoax.q2' files. Although the two time histories follow each other closely throughout the run, it can be seen that the direct method highlights fluctuations in the heating whereas the indirect method tends to smooth out these fluctuations.

The stagnation point heating-time history is shown with that of the Stanton number (from the '1Ddemocoax.q1' and '1Ddemocoax.ch1' files) in Figure 7. The Stanton number remains constant as is generally expected, and because of the small temperature rise during the run, so does the heat transfer rate. Note that the data shown in Figure 7 (and Figure 6) extends well beyond the semi-infinite test time estimated from Figure 2, which was approximately 1.5 seconds from the point at which heating began. Because the semi-infinite assumption was eventually violated, and because lateral conduction also began to become significant as the surface temperature increased, the one-dimensional analysis of the data became less accurate with time. This is why the Stanton number begins to increase slightly after the 4.5 second mark. In most cases (including this one), a sufficient amount of data can be acquired before the one-dimensional model is invalidated, and the later data are usually ignored. This portion of the run is shown here only to illustrate the limits of the applicability of the one-dimensional model.

The average values for the "democoax" data set of the indirect and direct method heat fluxes (from the '1Ddemocoax.dist1' and '1Ddemocoax.dist2' files) measured over the hemisphere are plotted in Figure 8, and as would be expected from the time histories in Figure 6, are nearly identical. Finally, in Figure 9 the averaged direct method heat transfer rate values are shown along with their standard deviations (both in the '1Ddemocoax.dist2' file); the small values of the standard deviations indicate that the data from this run are quite reliable.

The measured temperature-time histories of the thin-film gages on the 70° sphere-cone (twelve, distributed along a single ray at increments of $S/R_b = 0.1$) from the "demothin" data set are plotted in Figure 10. These data are found in the '1Ddemothin.t' file. Because the thin-film gages were mounted on an thermally insulative substrate (Macor) they experienced a much greater temperature rise than the coaxial thermocouples.

The time histories of the heat flux at the stagnation point gage ($S/R_b = 0$) as computed using both the direct and the indirect method are shown in Figure 11. These time-histories are found in the '1Ddemothin.q1' and '1Ddemothin.q2' files. Because of the large surface temperature rise the direct and indirect method heating-time histories do not remain constant as was the case for the coaxial thermocouples, but do again follow each other closely throughout the run. Because of this, an averaged heat transfer rate is a meaningless quantity. However, as shown in Figure 12, the Stanton number (from the '1Ddemothin.ch1" file) is nearly constant and can be averaged. To illustrate this point, consider the distributions plotted in Figures 13 and 14. Averaged heat transfer rates are plotted in Figure 13 and as expected, the average values changes with the window position. The average heat flux in the original window of 3.0 to 4.0 seconds (from '1Ddemothin.dist1' file) is different than that in a user-input (using option 3) window from 2.75 to 3.25 seconds (from the '1Ddemothin.dist1new') file. Both are different than the value extrapolated to a reference temperature of 300 °K (also in '1Ddemothin.dist1'). On the other hand, the averaged Stanton number values do not change with the averaging window, as shown in Figure 14. From these figures, it can be seen that while both the Stanton number and heat flux computations at a given time are valid, it is usually simpler to refer to the Stanton number since the heat transfer rate only makes sense if information on the wall

temperature is provided (or if the wall temperature rise is small in comparison to the stagnation temperature, as seen in the coaxial thermocouple data set).

The finite-volume data reduction options were also employed in the reduction of the 'demothin' data set. As shown in Figure 15, the direct and indirect method Stanton number-time histories, which are constant property solutions multiplied by an empirical correction factor, are in excellent agreement with the numerical solution (from the '1Ddemothin.q3' file) until well into the run when the semi-infinite approximation begins to become less accurate.

Temperature profiles through the substrate of the stagnation-point gage ("TF19") from the finite-volume solution at various times during the run are shown in Figure 16 (these data are from the '1Ddemothin.TF19' file, which was created using option 9). In Figure 16, note that at 3.5 seconds, the temperature at the back-face has begun to rise. The back-face temperature is one indicator of the validity of the semi-infinite substrate model. When the back-face temperature rise begins to become significant (relative to the sensor temperature) the semi-infinite model does not apply, since a constant back-face temperature is assumed in this model. The back-face temperature-time histories for each gage are located in the '1Ddemothin.tback' file; these data are plotted for several gages in Figure 17.

FINITE-VOLUME APPLICATIONS

Use of the finite-volume options in the 1DHEAT code makes it possible to analyze problems for which the classical semi-infinite substrate model (indirect or direct method) is not applicable. Specifically, the 1DHEAT code can be used to reduce data from gages with substrates of finite thickness, and these substrates may be comprised of one of more layers of different materials. Although the limiting assumption of one-dimensional conduction still applies in these cases, the finite-volume approach represents the actual physics of the problem more accurately than the semi-infinite substrate model.

In Figure 18, the heating distribution on a 70° sphere-cone similar to the one in the "demothin" data set is plotted for a test in the Langley 20" Mach 6 Air Tunnel (ref. 16). The distributions shown in Figure 18 are from analysis by the indirect, semi-infinite substrate method and by the finite-volume method. In this example (courtesy Thomas Horvath, NASA Langley), the model was 6" in diameter and was machined from chromel and instrumented with Type-E coaxial thermocouples. This model was designed for testing in a shock tube with run times on the order of milliseconds, as opposed to the run times in the Mach 6 tunnel which were on the order of seconds. Testing in the Mach 6 tunnel led to the semi-infinite assumption being violated in the corner region of the model, where the chromel substrate was considerably thinner than for the rest of the model. Because of this, analysis by the semi-infinite method led to invalid results in the corner region. Results from the semi-infinite analysis showed that there was a broad local heating peak at the corner of the model, which was much greater than that of the 70° sphere-cone model in the "demothin" example. However, when the finite-volume model, which accounts for non-infinite

substrate thickness, was employed for data reduction, this peak was found to be considerably smaller, which made the distribution more consistent with the "demothin" data set.

Multiple-layer substrate results are illustrated in Figure 19 in which heating data from two 0.25" radius, 4" long cylinders tested separately in the NASA Langley 20" Mach 6 Air Tunnel is presented (courtesy Scott Berry, NASA Langley). The first cylinder was machined from Macor and instrumented with thin-film gages. A 0.002" layer of Upilex was applied to the second cylinder, which was also machined from Macor. This Upilex layer was instrumented with thin-film gages (note the tighter gage spacing possible on the Upilex, see the discussion on Upilex in Appendix C). When tested, both cylinders were aligned perpendicular to the freestream flow so that the thin-film gages, which were in a single row along the leading edge of each cylinder, measured the two-dimensional stagnation point heating along the length of each cylinder.

For the Upilex/Macor cylinder the thermal penetration depth during the test was much greater than the thickness of the Upilex layer, which made this a multiple-layer problem. Thus, the heat transfer was computed using the finite-volume technique, with 5 points in the Upilex layer (dx = 0.0102 mm) and with 244 points in the Macor layer (dx = 0.0260 mm). Figure 19 shows the comparison between the computed Stanton numbers on the Upilex/Macor cylinder with that from the all-Macor cylinder, for which data was reduced using the indirect, semi-infinite analytical method. The computed heat transfer coefficient (Stanton number) distributions for the two models, which were geometrically identical but had dissimilar thermal response characteristics due to the difference in substrate materials, are in close agreement both with each other and with the computed Fay-Riddell two-dimensional stagnation point Stanton number.

The temperature profile through the substrate of one of the gages on the Upilex/Macor cylinder at different times during the test is shown Figure 20. The discontinuity in the slope of the temperature profile at 0.0508 mm is the interface between the low thermal conductivity Upilex and the high (relative to Upilex) conductivity Macor.

CONCLUDING REMARKS

A FORTRAN computer code, 1DHEAT, has been developed for the reduction of heat transfer data from thin-film gages and coaxial thermocouples. This code incorporates both analytical and numerical techniques for the solution of the one-dimensional heat conduction problem. The analytical techniques are based on the constant thermal properties, semi-infinite substrate approximation. The effects of the variation of thermal properties with temperature are included through either a variable thermal conductivity, constant thermal diffusivity approximation, or through the use of an empirically-derived correction factor to the constant thermal properties solution. The numerical technique is a one-dimensional finite-volume discretization with variable substrate thermal properties. The finite-volume method adds the capability for heat transfer computations with a substrate comprised of multiple layers

of different materials or of finite wall thickness. Use of this code has been demonstrated with the reduction of sample experimental thin-film gage and coaxial thermocouple data sets.

REFERENCES

1. Vidal, Robert J., "Transient Surface Temperature Measurements," CAL Rep. NO. 114, Cornell Aeronautical Lab., Inc., March 1962.
2. Schultz, D. L. and Jones, T. V., "Heat Transfer Measurements in Short-Duration Hypersonic Facilities," AGARD-AG-165, Feb. 1973.
3. Cook, William J., "Unsteady Heat Transfer to A Semi-Infinite Solid With Arbitrary Surface Temperature History and Variable Thermal Properties," Iowa State University Technical Report ISU-ERI-AMES-67500, Feb. 1970.
4. Hartunian, R. A. and Varwig, R. L., "On Thin-Film Heat Transfer Measurements in Shock Tubes and Wind Tunnels," Phys. Fluids, vol. 5, no. 2, Feb. 1962, pp. 169-174.
5. Miller, C. G., "Comparison of Thin-Film Resistance Heat-Transfer Gages With Thin-Skin Transient Calorimeter Gages in Conventional Wind Tunnels," NASA TM 83197, Dec. 1981.
6. White, F. M., Heat and Mass Transfer, Addison-Wesley Publishing, New York, 1988.
7. Patankar, S. V., Numerical Heat Transfer and Fluid Flow, Hemisphere, New York, 1980.
8. Dunn, M. G., Rae, W. J., and Holt, J. L., "Measurement and Analysis of Heat-Flux Data in a Turbine Stage: Part I: Description of Experimental Apparatus and Data Analysis," ASME Journal of Engineering for Gas Turbines and Power, Vol. 106, Jan. 1984.
9. Pittman, C. M., and Brinkley, K. L., "One-Dimensional Numerical Analysis of the Transient Thermal Response of Multilayer Insulative Systems," NASA TMX-3370, 1976.
10. Bradley, P. F., and Throckmorton, D. A., "Space Shuttle Orbiter Flight Heating Rate Measurement Sensitivity to Thermal Protection System Uncertainties," NASA TM 83138, 1981.
11. Kendall, D. N., Dixon, W. Paul, and Schulte, Edward H., "Semiconductor Surface Thermocouples for Determining Heat-Transfer Rates," IEEE Transactions on Aerospace and Electronic Systems, vol. AES-3, no. 4, July 1967, pp. 596-603.
12. Hedlund, E. R, Hill, J. A. F., Ragsdale, W. C., and Voisinet, R. L. P., "Heat Transfer Testing in the NSWC Hypervelocity Wind Tunnel Utilizing Co-axial Surface Thermocouples," NSWC MP 80-151, March 1980.
13. Cook, William, J., "Determination of Heat-Transfer Rates from Transient Surface Temperature Measurements," AIAA J., vol. 8, no. 7, July 1970, pp. 1366-1368.
14. Cook, William, J., and Felderman, E. J., "Reduction of Data from Thin-Film Heat-Transfer Gages: A Concise Technique," AIAA J. vol. 4, no. 3, March 1966, pp. 561-562.
15. Hollis, B. R., and Perkins, J. N. "Hypervelocity Aeroheating Measurements in Wake of Mars Mission Entry Vehicle," AIAA Paper 95-2314, 1995.
16. Micol, J. R. "Hypersonic Aerodynamic/Aerothermodynamic Testing Capabilities at Langley Research Center: Aerothermodynamic Facilities Complex," AIAA Paper 95-2107, 1995.

17. Neumann, R. D. "CFD Code Validation - An Instrumentation Perspective," AIAA Paper 94-2541, 1994.
18. Touloukian, Y. S., and Buyco E. H., Thermophysical Properties of Matter; Volume 4. Specific Heat: Metallic Elements and Alloys, IFI/Plenum, New York, 1970.
19. Touloukian, Y. S., Powell, R. W., Ho, C. Y., and Klemens, P. G., Thermophysical Properties of Matter; Volume 1, Thermal Conductivity: Metallic Elements and Alloys, IFI/Plenum, New York, 1970.
20. Miller, C. G., "Experimental and Predicted Heating Distributions for Biconics at Incidence in Air at Mach 10," NASA TP 2334, Nov. 1984.
21. Wannenwetsch G. D., Ticatch, L. A., Kidd, C. T., and Arterbury, R. L., "Results of Wind Tunnel Tests Utilizing the Thin-Film Technique to Measure Wing Leading-Edge Heating Rates," AEDC-TR-83-50, May 1984.
22. Mentre, V. and Consigny, H., "An Improved Data Reduction Technique for Thin-Film Heat Transfer Measurements Using Surface Thermocouples or Thin-Films," ICIASF Record 1987, pp. 369-377.
23. Soos, Troy., "Thermal Conductivity and Thermal Diffusivity of Ceramic Materials," Holometrix Inc. Rep. NAS-80, December 1992.
24. Soos, Troy., "Thermal Conductivity and Thermal Diffusivity of Glass and Ceramic Materials," Holometrix Inc., Rep. NAS-82, June 1993.
25. Soos, Troy, "Thermal Conductivity and Thermal Diffusivity of Macor Ceramics," Holometrix Inc., Rep. NAS-83, June 1994.
26. Campell, R. C., "Thermal Diffusivity, Specific Heat, and Thermal Conductivity of Upilex, Macor, and Quartz," Holometrix Inc., Rep. NAS-84, Jan. 1995.
27. Fay, J. A., and Riddell, F. R., "Theory of Stagnation Point Heat Transfer in Dissociated Air," Journal of the Aeronautical Sciences, vol. 25, no. 2, Feb. 1958, pp.73-85.
28. McBride, B. J., Gordon, S., and Reno, M. A., "Coefficients for Calculating Thermodynamic and Transport Properties of Individual Species," NASA TM-4513, Oct. 1993.

APPENDIX A. ANALYTICAL HEAT TRANSFER MODELS

The governing equation for one-dimensional heat conduction in a semi-infinite solid with constant thermal properties can be expressed as (ref. 2)

$$\frac{\partial^2 \theta(x,t)}{\partial x^2} = \frac{1}{\alpha_0} \frac{\partial \theta(x,t)}{\partial t} \tag{A-1}$$

where

$$\theta(x,t) = T(x,t) - T(x,0) \tag{A-2}$$

with boundary conditions

$$\dot{q}(0,t) = -k_0 \frac{\partial \theta(0,t)}{\partial x} \tag{A-3}$$

$$\theta(\infty,t) = 0$$

$$\theta(x,0) = 0$$

This equation may be solved using Laplace transforms. The transformed differential equation is

$$\alpha_0 \mathcal{L}\left(\frac{\partial^2 \theta}{\partial x^2}\right) = \mathcal{L}\left(\frac{\partial \theta}{\partial t}\right) \tag{A-4}$$

with boundary conditions

$$\dot{q}(0,s) = -k_0 \frac{\partial \theta(0,s)}{\partial x} \tag{A-5}$$

$$\theta(\infty,s) = 0$$

$$\theta(x,0) = 0$$

where

$$\mathcal{L}[\theta(x,t)] \equiv \theta(x,s) \tag{A-6a}$$

$$\mathcal{L}[q(x,t)] \equiv q(x,s) \tag{A-6b}$$

The Laplace transforms of the derivatives are

$$\mathcal{L}(\frac{\partial\theta}{\partial t}) = s\mathcal{L}(\theta) - \theta(x,0) \tag{A-7}$$

and

$$\mathcal{L}(\frac{\partial^2\theta}{\partial x^2}) = \int_0^\infty e^{-st}\frac{\partial^2\theta}{\partial x^2}dt = \frac{\partial^2}{\partial x^2}\int_0^\infty e^{-st}\theta dt = \frac{\partial^2}{\partial x^2}\mathcal{L}(\theta) \tag{A-8}$$

Now, let

$$v = \mathcal{L}[\theta(x,t)] \tag{A-9}$$

then the transformed equation is

$$sv - \theta(x,0) = \alpha_0\frac{d^2v}{dx^2} \tag{A-10}$$

which has the general solution

$$v(x,s) = \mathcal{L}[\theta(x,t)] = Ae^{x\left(\frac{s}{\alpha_0}\right)^{\frac{1}{2}}} + Be^{-x\left(\frac{s}{\alpha_0}\right)^{\frac{1}{2}}} + \frac{\theta(x,0)}{s} \tag{A-11}$$

Application of the boundary conditions leads to

$$A = 0 \tag{A-12a}$$

$$B = \frac{\dot{q}(0,s)\sqrt{\alpha_0}}{k_0 s^{\frac{1}{2}}} \tag{A-12b}$$

then

$$\mathcal{L}[\theta(x,t)] = \frac{\dot{q}(0,s)}{\beta_0 s^{\frac{1}{2}}}e^{-x\left(\frac{s}{a}\right)^{\frac{1}{2}}} \tag{A-13}$$

where

$$\beta_o = \frac{k_0}{\sqrt{\alpha_0}} = \sqrt{\rho_0 c_{p,0} k_0} \tag{A-14}$$

which evaluated at the surface ($x=0$) gives

$$\mathcal{L}[\dot{q}(0,t)] = \dot{q}(0,s) = \beta_0 s^{\frac{1}{2}} \mathcal{L}[\theta(0,t)] \tag{A-15}$$

or by the ($t=0$) boundary condition in (A-3)

$$\dot{q}(0,s) = \frac{\beta_0}{\sqrt{s}} \left\{ s\mathcal{L}[\theta(0,t)] - s\theta(0,0) \right\} \tag{A-16}$$

then

$$\dot{q}(0,s) = \frac{\beta_0}{\sqrt{s}} \mathcal{L}\left[\frac{d\theta}{dt}(0,t) \right] \tag{A-17}$$

The Laplace transform of the system can then be inverted through a convolution to obtain an expression for surface heat transfer as a function of time

$$\dot{q}(0,s) = \frac{\beta_0}{\sqrt{\pi}} \mathcal{L}\left(\frac{1}{t} \right) \mathcal{L}\left(\frac{d\theta}{dt}(0,t) \right) \tag{A-18}$$

$$\mathcal{L}^{-1}[\dot{q}(0,s)] = \dot{q}(0,t) = \frac{\beta_0}{\sqrt{\pi}} \int_0^t \frac{\frac{d\theta}{d\lambda}(0,\lambda)}{\sqrt{t-\lambda}} d\lambda \tag{A-18}$$

This equation can be simplified through integration by parts as

$$\int_{\lambda_1}^{\lambda_2} u dv = uv\Big|_{\lambda_1}^{\lambda_2} - \int_{\lambda_1}^{\lambda_2} v du$$

where

$u = u(\lambda)$

$v = v(\lambda)$ (A-20)

where

$$u = \frac{1}{\sqrt{t-\lambda}} \tag{A-21a}$$

$$du = \frac{d\lambda}{2(t-\lambda)^{\frac{3}{2}}} \tag{A-21b}$$

and

$$dv = \frac{d\theta}{d\lambda} d\lambda \tag{A-22a}$$

$$v = \theta(0,\lambda) \tag{A-22b}$$

An arbitrary constant can be added to v without changing dv. This is done in order to avoid a singularity later in the derivation.

$$dv = \frac{d\theta}{d\lambda} d\lambda \tag{A-23a}$$

$$v = \theta(0,\lambda) - \theta(0,t) \tag{A-23b}$$

then

$$\dot{q}(t) \equiv \dot{q}(0,t) = \frac{\beta_0}{\sqrt{\pi}} \left[\frac{\theta(0,t)}{\sqrt{t}} + \frac{1}{2} \int_0^t \frac{\theta(0,t) - \theta(0,\lambda)}{(t-\lambda)^{\frac{3}{2}}} d\lambda \right] \tag{A-24}$$

In order to avoid the singularity at (t=l), Cook and Felderman (ref. 14) reduce the integral to a summation by approximating the temperature as a piecewise linear function

$$\theta(0,\lambda) \equiv \overline{\theta(\lambda)} = \theta(t_{i-1}) + \frac{\theta(t_i) - \theta(t_{i-1})}{\Delta t} (\lambda - t_{i-1}) \tag{A-25}$$

Then by transforming the integral into a summation of discrete integrals

$$\frac{\sqrt{\pi}}{\beta_0} \dot{q} = \frac{\theta_n}{\sqrt{t_n}} + \frac{1}{2} \sum_{i=1}^{i=n} \left\{ (\theta_n - \theta_{i-1}) \int_{t_{i-1}}^{t_i} \frac{d\lambda}{(t_n - \lambda)^{\frac{3}{2}}} - \frac{(\theta_i - \theta_{i-1})}{\Delta t} \int_{t_{i-1}}^{t_i} \frac{\lambda - t_i}{(t_n - \lambda)^{\frac{3}{2}}} d\lambda \right\} \tag{A-26}$$

with integration by parts of the second integral

$$\frac{\sqrt{\pi}}{\beta_0}\dot{q} = \frac{\theta_n}{\sqrt{t_n}} + \frac{1}{2}\sum_{i=1}^{i=n}\left\{(\theta_n - \theta_{i-1})\left[\frac{2}{(t_n-\lambda)^{\frac{1}{2}}}\right]_{t_{i-1}}^{t_i} - \frac{(\theta_i - \theta_{i-1})}{\Delta t}\left[\frac{2(\lambda - t_{i-1})}{(t_n-\lambda)}\right|_{t_{i-1}}^{t_i} - \int_{t_{i-1}}^{t_i}\frac{d\lambda}{(t_n-\lambda)^{\frac{1}{2}}}\right]\right\} \tag{A-27}$$

evaluation of the all terms gives

$$\frac{\sqrt{\pi}}{\beta_0}\dot{q} = \frac{\theta_n}{\sqrt{t_n}} + \sum_{i=1}^{i=n}\left\{\frac{\theta_n - \theta_i}{(t_n - t_i)^{\frac{1}{2}}} - \frac{\theta_n - \theta_{i-1}}{(t_n - t_{i-1})^{\frac{1}{2}}} + \frac{2(\theta_i - \theta_{i-1})}{(t_n - t_i)^{\frac{1}{2}} + (t_n - t_{i-1})^{\frac{1}{2}}}\right\} \tag{A-28}$$

The first term in the summation is undefined at (i=n). However, by l'Hopital's rule, the limit as i approaches n of this term is zero.

With the condition that $\theta(t_0) = 0$ where $t_0 = 0$, the summations can be separated to get

$$\frac{\sqrt{\pi}}{\beta_0}\dot{q} = \sum_{i=1}^{i=n-1}\frac{\theta_n - \theta_i}{(t_n - t_i)^{\frac{1}{2}}} - \sum_{i=2}^{i=n}\frac{\theta_n - \theta_{i-1}}{(t_n - t_{i-1})^{\frac{1}{2}}} + 2\sum_{i=1}^{i=n}\frac{2(\theta_i - \theta_{i-1})}{(t_n - t_i)^{\frac{1}{2}} + (t_n - t_{i-1})^{\frac{1}{2}}} \tag{A-29}$$

Finally, the indices on the second summation are shifted to get

$$\dot{q}(t_n) = \frac{2\beta_0}{\sqrt{\pi}}\sum_{i=1}^{n}\frac{\theta_i - \theta_{i-1}}{\sqrt{t_n - t_i} + \sqrt{t_n - t_{i-1}}} \tag{A-30}$$

Equation (A-1) is valid only when the variation in the thermal properties can be neglected, that is, when the temperature rise is small. In hypersonic heat transfer experiments the temperature rise is usually quite large, therefore, the variation in the thermal properties must be accounted for in the heat transfer model.

For some materials, such as the metals in a coaxial thermocouple, the thermal conductivity increases rapidly with temperature, but the thermal diffusivity increases only slightly. Thus the relationship between heat flux and temperature for a coaxial thermocouple can be approximated using the approach suggested by Cook (ref. 3), in which the thermal conductivity is allowed to vary, but the diffusivity is held constant. The dependent variable is transformed by

$$\phi = \int_0^{\theta}\frac{k}{k_0}d\theta \tag{A-31}$$

which leads to the system

$$\frac{\partial^2 \phi(x,t)}{\partial x^2} = \frac{1}{\alpha_0} \frac{\partial \phi(x,t)}{\partial t} \tag{A-32}$$

The form of equation (A-30) is identical to that of equation (A-1). Thus, it has the solution

$$\dot{q}(t_n) = \frac{2\beta_0}{\sqrt{\pi}} \sum_{i=1}^{n} \frac{\phi_i - \phi_{i-1}}{\sqrt{t_n - t_i} + \sqrt{t_n - t_{i-1}}} \tag{A-33}$$

For insulative materials such as Macor and quartz, which are used as substrates for thin-film gages, temperature has a strong effect on both the thermal conductivity and the thermal diffusivity. Thus, neither (A-1) nor (A-32) are valid representations of the relationship between heat flux and temperature. It has been found however, that accurate correction factors for the effects of variable thermal properties can be determined which can be applied to the constant properties solution . The corrected equation takes the form of

$$\dot{q}_{\beta(T)} = \dot{q}_{\beta_0} [1 + \beta' \Delta T_s] \tag{A-34}$$

where the constant property solution can be obtained using the direct method of equation (5) or the indirect method of equation (7).

The correction factors are derived from heat transfer rates computed using the finite-volume technique. The finite-volume technique is discussed in Appendix B, while the derivation of the correction factors is presented in Appendix C. These corrected semi-infinite substrate heat transfer results are typically within a few percent of the results from the more rigorous finite-volume computations. The advantage of this technique is the simplicity with which the numerical summations in equations (5,7) can be calculated and then corrected for property variations by equation (12). In contrast, the finite-volume solution generally requires more time due to the need to construct a finite-volume input file and to analyze the effects of grid spacing on the computations. For this reason it is less useful for "real-time" data analysis during wind tunnel testing. However, the finite-volume method is still very valuable in that it involves no empiricism, the empirical correction factors for the analytical method are derived from it, and it is the only way to correctly solve the finite wall thickness problem or the multiple-layer substrate problem. It is thus suggested that the analytical semi-infinite methods be employed to quickly reduce data during a test series, and then later that a more rigorous analysis be carried out using the finite-volume technique.

APPENDIX B. FINITE-VOLUME HEAT TRANSFER MODEL

In theory, the most accurate method for computation of heat flux in a solid body would be through the use of a three-dimensional finite-volume technique to compute the temperature distribution inside the body in question. In this manner, the effects of the variation in thermal properties with temperature, as well as those of lateral and transverse heat conduction could be taken into account. However, it would in practice be very difficult to instrument a model with enough sensors to accurately measure the entire surface temperature distribution, which would be required as a boundary condition for a computational solution. The computational time would also be much greater for a three-dimensional solution, and considerable time would be required to generate a three-dimensional computational grid and perform a grid resolution study. While accurate, miniaturized temperature sensors and powerful computational resources are available today, and thus a three-dimensional computation can be performed, this is not a practical approach for a real-time analysis code which can be applied to generic configurations with a minimum of preparatory work. For these reasons, the numerical model is presently restricted to that of one-dimensional heat conduction.

An implicit finite-volume discretization is implemented in 1DHEAT. The geometry and notation for this model are shown in Figure 21. The temperature distribution within the solid can be obtained from an energy balance within each cell:

$$\dot{q}_{in} - \dot{q}_{out} = \dot{q}_{stored} \tag{B-1}$$

which by a time-implicit, finite-volume discretization yields

$$\left[-k_l \frac{(T_i^n - T_{i-1}^n)}{(x_i - x_{i-1})}\right] - \left[-k_r \frac{(T_{i+1}^n - T_i^n)}{(x_{i+1} - x_i)}\right] = \left[(\rho c_p)_i \frac{(T_i^n - T_i^{n-1})}{\Delta t}\right] \Delta x_i \tag{B-2}$$

or by rearrangement

$$T_{i-1}^n \left[k_l\right] + T_i^n \left[-k_l - k_r \frac{(x_i - x_{i-1})}{(x_{i+1} - x_i)} - (\rho c_p)_i (x_i - x_{i-1}) \frac{\Delta x_i}{\Delta t}\right] + T_{i+1}^n \left[k_r \frac{(x_i - x_{i-1})}{(x_{i+1} - x_i)}\right] = \left[(\rho c_p)_i (x_i - x_{i-1}) \frac{\Delta x_i}{\Delta t}\right] T_i^{n-1} \tag{B-3}$$

This model is second-order accurate in space and first-order in time. Note that all material properties values in the coefficients of T are lagged and evaluated at the $(n\text{-}1)$ level. Equation (B-3) is valid for the computational cells

on the interior of the domain. The temperatures at the exterior and interior (it is assumed that the actual wind tunnel model is hollow in order to allow space for the sensor wires) of the domain are functions of the boundary conditions.

The temperature of the first computational node is extrapolated from the temperature measured on the external face of the model by the sensor (Figure 22a.):

$$T_1^n = \frac{2}{3}\left(T_{gage}^n + \frac{1}{2}T_2^n\right) \tag{B-4}$$

By substitution into equation (B-3), the temperature at node 2 is

$$T_2^n\left[-k_{l,2} - k_{r,2}\frac{(x_2 - x_1)}{(x_3 - x_2)} - (\rho c_p)_2(x_2 - x_1)\frac{\Delta x_2}{\Delta t} + \frac{1}{3}k_{l,2}\right] + T_3^n\left[k_{r,2}\frac{(x_2 - x_1)}{(x_3 - x_2)}\right] = \left[(\rho c_p)_2(x_2 - x_1)\frac{\Delta x_2}{\Delta t}T_2^{n-1} - \frac{2}{3}T_{gage}^n\right] \tag{B-5}$$

Several boundary conditions for the back surface are possible: adiabatic surface, constant temperature, and measured temperature. The measured temperature boundary condition would be the most accurate, but since it is not usually practical to make this measurement, the adiabatic surface boundary condition is generally used. The rationale for this boundary condition is that the heat conduction to the stagnant gas in the hollow interior of the model is negligible in comparison to the heat flux through the solid. At current, the constant temperature and adiabatic surface boundary conditions, but not the measured temperature boundary condition, are implemented in 1DHEAT. These boundary conditions are illustrated in Figure 22b.

The adiabatic boundary condition is implemented by setting $\dot{q}_{out}$ to zero in equation (B-1) for the *(m-1)th* computational node

$$T_{m-2}^n\left[k_{m-1}\right] + T_{m-1}^n\left[-k_{l,m-1} - (\rho c_p)_{m-1}(x_{m-1} - x_{m-2})\frac{\Delta x_{m-1}}{\Delta t}\right] = \left[(\rho c_p)_{m-1}(x_{m-1} - x_{m-2})\frac{\Delta x_{m-1}}{\Delta t}\right]T_{m-1}^{n-1} \tag{B-6}$$

For the constant interior surface temperature boundary condition, the temperature at the *mth* node is extrapolated from the surface by

$$T_m^n = \frac{2}{3}\left(T_{back}^n + \frac{1}{2}T_{m-1}^n\right) \tag{B-7}$$

Then by substitution into (B-3)

$$T^n_{m-2}\left[k_{l,m-1}\right]+T^n_{m-1}\left[-k_{l,m-1}-k_{r,m-1}\frac{(x_{m-1}-x_{m-2})}{(x_m-x_{m-1})}-(\rho c_p)_{m-1}(x_{m-1}-x_{m-2})\frac{\Delta x_{m-1}}{\Delta t}+\frac{1}{3}k_{r,m-1}\frac{(x_{m-1}-x_{m-2})}{(x_m-x_{m-1})}\right]$$
$$=\left[(\rho c_p)_{m-1}(x_{m-1}-x_{m-2})\frac{\Delta x_{m-1}}{\Delta t}T^{n-1}_{m-1}-\frac{2}{3}k_{r,m-1}\frac{(x_{m-1}-x_{m-2})}{(x_m-x_{m-1})}T_{back}\right] \tag{B-8}$$

The system of equation (B-3) with boundary conditions of equations (B-5), and (B-6) or (B-8) forms a tridiagonal matrix of unknowns which can rapidly be solved using the Thomas algorithm.

The finite-volume technique in 1DHEAT can be also used to solve the one-dimensional heat conduction equation in a substrate with up to three substrate layers in which material thickness, grid spacing, and thermal properties are different in each layer. The number of layers can be increased simply by changing the dimensions in the code.

Note that in a multiple-layer problem the thermal conductivities on either side of the interface may be discontinuous. Because of this, it is not consistent to extrapolate the cell interface thermal conductivities, k_l and k_r, by averaging the conductivities of the adjacent nodes, that is

$$k_{l,i}=\frac{k_{i-1}+k_i}{2} \tag{B-9}$$

As proof, consider a material in which one layer was a perfect insulator *(k = 0)* and the other material of the other layer had some non-zero conductivity. At the interface of the two materials, the thermal conductivity from equation (B-8) would be non-zero, permitting heat transfer into the insulated layer.

The interface conductivity is properly defined through the series electrical resistor analogy (ref. 6). The heat transfer at the interface is given by

$$q_{\text{int}}=\frac{-\Delta T}{\sum R}=\left(-k_{\text{int}}\frac{\Delta T}{\Delta x}\right)A_x \tag{B-10}$$

where R is defined as the conduction resistance

$$R_i=\frac{1}{k_i\int_{x_A}^{x_B}\frac{dx}{A_x}} \tag{B-11}$$

In 1DHEAT, the cell wall areas are constant. From the notation in Figure 21, the conduction resistances between the nodes and the interface are:

$$R_{i-1} = \frac{1}{k_{i-1}\frac{\Delta x_{i-1}}{2A_x}} \tag{B-12a}$$

$$R_i = \frac{1}{k_i \frac{\Delta x_i}{2A_x}} \tag{B-12b}$$

Then from equation (B-10)

$$k_{\text{int}} = \frac{\frac{x_i - x_{i-1}}{A_x}}{R_{i-1} + R_i} = \frac{\frac{x_i - x_{i-1}}{A_x}}{\frac{k_{i-1}\Delta x_{i-1}}{2A_x} + \frac{k_i \Delta x_i}{2A_x}} \tag{B-13}$$

By defining

$$F_i = \frac{(\Delta x_i)/2}{x_i - x_{i-1}} \tag{B--14}$$

equation (B-13) becomes

$$k_{l,,i} = \frac{1}{\frac{1-F_i}{k_{i-1}} + \frac{F_i}{k_i}} \tag{B-15}$$

With this definition, the interface thermal conductivity in the above example would have the proper value of zero. This formulation is also useful in that it permits the node spacing to differ from layer-to-layer, although in the 1DHEAT code it is uniform within a layer.

The approximate grid Fourier number based on constant material thermal properties is

$$\sigma = \frac{\alpha_0 \Delta t}{(\Delta x)^2} \tag{B-15}$$

Because this is an implicit formulation there are no stability restrictions on σ, and the grid spacing Δx may be adjusted as desired to make trade-offs between solution accuracy and computational time. The grid spacings are varied separately by specifying the number of mesh points in each layer in the finite-volume set-up file. It may be advisable to adjust the grid spacings so that the Fourier numbers in each layer are identical, although limited investigations have not shown any significant effects of varying σ from layer to layer.

APPENDIX C. MATERIAL THERMAL PROPERTIES

The accuracy of the material thermal property data is a crucial, but often neglected, factor in the reduction of experimental heat transfer data. Since material properties can rarely be considered to remain constant, their dependence on temperature must be known, and must be accounted for in the data reduction scheme. The effects of thermal properties can be rigorously dealt with by employing a finite-volume data reduction method as detailed in Appendix B, or in a simpler empirical manner by the application of correction factors to an analytical constant properties solution. However, even if the correct theoretical models are used, it is extremely difficult to obtain accurate thermal property data for use in those models. Material handbooks generally only give data at a single point (usually room temperature). Thermal property data in the aerospace literature is also lacking, and what data exists is often contradictory.

While useful qualitative information can still be obtained, it is simply not possible to make quantitative conclusion from experiments without accurate thermal properties data. This is especially significant in regards to CFD code calibration exercises, as discussed by Neumann (ref. 17). Therefore, the thermal properties data incorporated into the 1DHEAT code are presented here along with a survey of data sources. It should be noted that thermal properties data in 1DHEAT are in some cases different than those published elsewhere. These thermal properties represents the best data currently available to the author, but are subject to change and should not be considered as THE definitive set of thermal properties data. This data may be modified by the user or data for other materials may be added to the 1DHEAT code as discussed at the end of this appendix. Comparisons between experimental results based on these properties and computational results are included at the end of this Appendix.

MATERIAL PROPERTY CURVE FITS

A summary of room-temperature properties of the materials for which data has been incorporated into 1DHEAT (chromel, constantan, Macor, quartz, Pyrex, 17-4 stainless steel, and Upilex) is given in Table 4. Curve fits for the variations in thermal properties with temperature are given in the respective sections of this appendix for each material. These curve fits are all considered to be valid for temperatures up to 600 °K.

Type-E Thermocouple

The Type-E chromel-constantan thermocouple manufactured by Medtherm is composed primarily (80-90% by volume) of chromel. Because of this, and because of the uncertainty in constantan thermal properties, it is recommended that the chromel curve fits of equation (C-1) be used to represent the Type-E thermocouple.

Chromel

Because chromel is a metal, it has high thermal conductivity and thus experiences a relatively low temperature rise (compared to an insulator) when exposed to heating. The effects of variable material thermal properties are thus less significant. However, there is a trade-off in that metals also have higher thermal diffusivity, and thus the time for which the semi-infinite approximation is valid is much shorter.

Chromel thermal property curve fits are presented in Figures 23a-23e. Chromel specific heat data are taken from Touloukian et al (ref. 18), which was the only source found for variation of chromel specific heat with temperature. Chromel thermal conductivity data was taken from Touloukian et al (ref. 19), Hoskins[1] (a supplier of chromel alloy) and from Medtherm[2] (a manufacturer of the Type-E thermocouples). Thermal diffusivity and thermal product values were computed from these data. Material property curve fits based on these data are:

$$\rho = 8714 \ (kg/m^3) \tag{C-1a}$$

$$c_p = 386.25 + 0.23981 \cdot T \ (J/kg\text{-}^\circ K) \tag{C-1b}$$

$$k = 11.845 + 1.9132 \cdot 10^{-2} \cdot T \ (W/m\text{-}^\circ K) \tag{C-1c}$$

$$\alpha = 3.5995 \cdot 10^{-6} + 2.9656 \cdot 10^{-9} \cdot T - 9.1293 \cdot 10^{-13} \cdot T^2 \ (m^2/s) \tag{C-1d}$$

$$\beta = 6398.4 + 6.6331 \cdot T \ (W\text{-}s^{1/2}/m^2\text{-}^\circ K) \tag{C-1e}$$

Constantan

Constantan thermal properties were obtained from the same sources as chromel properties. However, less data were available in these references and the curve fits below are of higher uncertainty than those for chromel. Constantan thermal properties curve fits are:

$$\rho = 8906 \ (kg/m^3) \tag{C-2a}$$

$$c_p = 318.54 + 0.25745 \cdot T \ (J/kg\text{-}^\circ K) \tag{C-2b}$$

$$k = 8.5591 + 4.6562 \cdot 10^{-2} \cdot T \ (W/m\text{-}^\circ K) \tag{C-2c}$$

$$\alpha = 3.1797 \cdot 10^{-6} + 1.1966 \cdot 10^{-8} \cdot T - 4.5508 \cdot 10^{-12} \cdot T^2 \ (m^2/s) \tag{C-2d}$$

$$\beta = 5336.2 + 11.754 \cdot T \ (W\text{-}s^{1/2}/m^2\text{-}^\circ K) \tag{C-2e}$$

These curve fits are plotted in Figures 24a-24e.

Macor

Macor is a machinable glass ceramic manufactured by the Corning[3] company. Macor is a thermal insulator, which makes it a good substrate material for thin-film gages because insulators have longer semi-infinite test times. However, temperature has a strong influence on the thermal properties of Macor, which complicates the

1 Hoskins Manufacturing Company, Detroit MI 48208
2 Medtherm Corporation, Huntsville, AL 35804
3 Corning Incorporated - Advanced Materials Department, Corning, NY 14831. Macor is a trademark of Corning Inc.

analysis of heat transfer data. Furthermore, the variation with temperature is not well documented. Thermal property data has been assembled from a number of sources, most of which are not in good agreement with each other. Macor thermal properties data were obtained from Corning, Miller at the NASA Langley Research Center (refs. 5,20), Wannenwetsch et al at the Arnold Engineering Development Center (ref. 21), CALSPAN (cited in ref. 5), Mentre and Consigny (ref. 22) and Soos (refs. 23-25) and Campell (ref. 26) at the Holometrix[4] company . The merits of each data set can be assessed from study of the references cited. Ultimately, Macor thermal property curve fits were based on references 23-25 and 26 because these data are recent (1992-1995), are repeatable, and cover a large range of temperatures.

Macor thermal properties curve fits are :

$$\rho = 2543.84 - 8.0 \cdot 10^{-12} \quad (kg/m^3) \tag{C-3a}$$

$$c_p = 114.04 + 2.5196 \cdot T - 1.5136 \cdot 10^{-3} \cdot T^2 \quad (J/kg\text{-}^\circ K) \tag{C-3b}$$

$$k = 0.33889 + 7.4682 \cdot 10^{-3} \cdot T - 1.6118 \cdot 10^{-5} \cdot T^2 + 1.2376 \cdot 10^{-8} \cdot T^3 \quad (W/m\text{-}^\circ K) \tag{C-3c}$$

$$\alpha = 1.3003 \cdot 10^{-6} - 2.2523 \cdot 10^{-9} \cdot T + 1.8571 \cdot 10^{-12} \cdot T^2 \quad (m^2/s) \tag{C-3d}$$

$$\beta = 754.2 + 3.7201 \cdot T - 2.4883 \cdot 10^{-3} \cdot T^2 \quad (W\text{-}s^{1/2}/m^2\text{-}^\circ K) \tag{C-3e}$$

Macor thermal properties are plotted in Figures 25a-25e.

Quartz

Like Macor, quartz is a thermal insulator and is thus also a good substrate material for thin-film gages. The main drawback to quartz is that it is a more difficult material to machine than Macor. Quartz thermal property data were obtained from Corning, GE[5] , NASA (ref. 5) and Holometrix (refs. 23, 26) and are presented in Figures 26a-26e. The curve fits presented are based on data from Holometrix for the same reasons as discussed in the section on Macor.

The curve fits for quartz thermal properties are:

$$\rho = 2192.5 \quad (kg/m^3) \tag{C-4a}$$

$$c_p = 197.85 + 1.9893 \cdot T - 7.3896 \cdot 10^{-4} \cdot T^2 \quad (J/kg\text{-}^\circ K) \tag{C-4b}$$

$$k = 0.96157 + 9.5491 \cdot 10^{-4} \cdot T + 5.5465 \cdot 10^{-7} \cdot T^2 \quad (W/m\text{-}^\circ K) \tag{C-4c}$$

$$\alpha = 1.5191 \cdot 10^{-6} - 4.136 \cdot 10^{-9} \cdot T + 7.2707 \cdot 10^{-12} \cdot T^2 - 4.4242 \cdot 10^{-15} \cdot T^3 \quad (m^2/s) \tag{C-4d}$$

$$\beta = 805.48 + 2.1192 \cdot T \quad (W\text{-}s^{1/2}/m^2\text{-}^\circ K) \tag{C-4e}$$

4 Holometrix Incorporated, Bedford, MA 01730-2323
5 GE Quartz Products, Cleveland, OH 44117

Pyrex

Like quartz and Macor, Pyrex[6] is another insulative material used as a thin-film gage substrate. The curve fits presented here are from reference 5 and are presented in Figures 27a-27e. Because Pyrex thermal properties vary much more with temperature than those of other materials, and it is not easily machined, it is generally not a preferred substrate choice.

$$\rho = 2227.0 \ (kg/m^3) \tag{C-5a}$$

$$c_p = -85.414 + 4.2839 \cdot T - 5.7482 \cdot 10^{-3} \cdot T^2 + 3.1047 \cdot 10^{-6} \cdot T^3 \ (J/kg\text{-}^\circ K) \tag{C-5b}$$

$$k = 1.5146 - 5.9068 \cdot 10^{-3} \cdot T + 1.8165 \cdot 10^{-5} \cdot T^2 \ (W/m\text{-}^\circ K) \tag{C-5c}$$

$$\alpha = 1.0622 \cdot 10^{-6} - 3.0254 \cdot 10^{-9} \cdot T + 7.3053 \cdot 10^{-12} \cdot T^2 \ (m^2/s) \tag{C-5d}$$

$$\beta = 541.63 + 2.0121 \cdot T + 4.3415 \cdot 10^{-3} \cdot T^2 \ (W\text{-}s^{1/2}/m^2\text{-}^\circ K) \tag{C-5e}$$

Upilex

A technique currently being developed at NASA Langley is the application of thin-film gages to a layer of Upilex film which is then applied to a wind tunnel model. Upilex is a thin (1 to 5 mil thickness) polyamide film manufactured by Ube[7] which has very low thermal conductivity and a highly finished surface. Because of the surface quality of the film, it is possible to obtain higher gage quality and spatial resolution than with other substrate materials. However because the Upilex is so thin, it usually cannot be treated as a semi-infinite substrate, and thus the finite-volume method must be used to carry out a multiple-layer analysis which takes into account both the Upilex surface layer and the sub-layer (typically Macor). Because this is a relatively new material, there is little data available on the thermal properties. Curve fits given below are based on data from Ube and Holometrix (ref 26) and should be considered as preliminary. These curve fits are plotted in Figures 28a-28e

$$\rho = 1490.0 \ (kg/m^3) \tag{C-6a}$$

$$c_p = -2258.2 + 19.492 \cdot T - 3.7267 \cdot 10^{-2} \cdot T^2 + 2.7812 \cdot 10^{-5} \cdot T^3 \ (J/kg\text{-}^\circ K) \tag{C-5b}$$

$$k = -0.26918 + 3.6348 \cdot 10^{-3} \cdot T - 7.2432 \cdot 10^{-6} \cdot T^2 + 5.0056 \cdot 10^{-9} \cdot T^3 \ (W/m\text{-}^\circ K) \tag{C-6c}$$

$$\alpha = 5.9629 \cdot 10^{-7} - 2.2994 \cdot 10^{-9} \cdot T + 4.2071 \cdot 10^{-12} \cdot T^2 - 2.8011 \cdot 10^{-15} \cdot T^2 \ (m^2/s) \tag{C-6d}$$

$$\beta = -1068.7 + 10.619 \cdot T - 2.0458 \cdot 10^{-2} \cdot T^2 + 1.4544 \cdot 10^{-5} \cdot T^3 (W\text{-}s^{1/2}/m^2\text{-}^\circ K) \tag{C-6e}$$

17-4 Stainless Steel

A technique sometimes utilized for wind tunnel model construction is to fabricate a model from steel, aluminum, or other easily machinable material. Sections are then cut out from the model and replaced with instrumented inserts. These inserts are typically Macor, quartz or Pyrex substrates with thin-film gages. Ideally, the substrates are thick enough that they can be considered as semi-infinite. However, this problem can be analyzed as a

6 Pyrex is a trademark of Corning Inc.
7 Ube Industries, New York, NY 10103

multiple-layer problem using the finite-volume technique. Thermal property data for 17-4 stainless steel obtained from ARMCO[8] is thus given here for use in a multiple-layer analysis. However, this data should only be taken as an example of metallic substrate properties since there are many varieties of steel or other metals which can be employed in model construction.

$$\rho = 7800 \ (\mathrm{kg/m^3}) \tag{C-7a}$$

$$c_p = 460 \ (\mathrm{J/kg\text{-}^\circ K}) \tag{C-7b}$$

$$k = 11.63 + 1.4816 \cdot 10^{-2} \cdot T \ (\mathrm{W/m\text{-}^\circ K}) \tag{C-7c}$$

$$\alpha = 3.2414 \cdot 10^{-6} + 4.1293 \cdot 10^{-9} \cdot T \ (\mathrm{m^2/s}) \tag{C-7d}$$

$$\beta = 6601.2 + 3.3208 \cdot T \ (\mathrm{W\text{-}s^{1/2}/m^2\text{-}^\circ K}) \tag{C-7e}$$

CORRECTION FACTORS

The numerical method discussed in Appendix B can be used to obtain an "exact" solution to the problem of one-dimensional transient heat conduction in a solid with variable thermal properties. However, this is not considered to be the optimal method for real-time reduction of large amounts of data because the finite-volume method generally requires more set-up work and analysis than the analytical method. This makes it somewhat less user-friendly, because non-experimental factors such as grid resolution and boundary conditions must be considered before the 1DHEAT code can be used to reduce data. The preferred methods for real-time data reduction are the semi-infinite substrate methods of equations (5) or (7) with the correction for variation of material properties with temperature of equation (12) for thin-film gages, and the semi-infinite substrate methods of equations (9) or (10) for coaxial thermocouples. The finite-volume method should be used to reduce selected sets of data to verify these results.

Correction factors for Macor were derived in a manner similar to Cook (ref. 3) and have the form

$$\dot{q}_{\beta(T)} = \dot{q}_{\beta_0}[1 + \beta' \Delta T_s] \tag{C-8}$$

The correction factor, β', for Macor was determined by comparing the computed heat transfer rates for a parabolic temperature-time history, $T = T(t^{1/2})$, (corresponding to a constant heat transfer rate for a substrate with constant thermal properties) for a substrate with thermal properties held constant to a substrate with variable thermal properties. In both cases the heat transfer rates were computed using the finite-volume method. These heat transfer rates are plotted versus temperature rise in Figure 29. The correction factor shown can be derived from this figure as

8 Armco Stainless Steel Products, Baltimore, MD 21203

$$\beta'(\Delta T_s) = \frac{\left(\frac{\dot{q}_{\beta(T)}}{\dot{q}_{\beta_0}} - 1\right)}{\Delta T_s} \tag{C-9}$$

The correction factor is considered to be valid for temperatures up to 600 °K and is implemented in 1DHEAT using the linear fit shown.

$$\beta' = 7.380 \cdot 10^{-4} - 4.604 \cdot 10^{-7} \cdot \Delta T_s \tag{C-10}$$

Note that although the linear fit is less accurate at lower temperatures (the computed correction factor goes to zero at room temperature) the actual correction to the heat transfer rate is the correction factor times the temperature rise, and the error is thus negligible at low temperatures.

The finite-volume solutions for constant and variable thermal properties and the corrected analytical solution are plotted in Figure 30 as a function of time. For this parabolic time history, the agreement is excellent. Although the correction factor values are derived only from this parabolic temperature-time history, they appear to be valid for any temperature-time relationship within the temperature range given for the material property curve fits. A sample comparison between corrected analytical results and finite-volume results is shown in Figure 31 (stagnation point heating from the "demothin" data set) and the agreement is excellent.

The correction factor for quartz was derived in the same manner as for Macor. The thermal properties for Pyrex in (C-5) are taken from reference 5, so the same correction factor is used.

For quartz, the correction factor is

$$\beta' = 9.414 \cdot 10^{-4} - 8.018 \cdot 10^{-8} \cdot \Delta T_s \tag{C-11}$$

The correction factor for Pyrex is a constant:

$$\beta' = 2.33 \cdot 10^{-3} \tag{C-12}$$

No correction factors were determined for the metallic materials or for Upilex. For the metals, the surface temperature rises experienced are generally small enough that the constant diffusivity approximation (eq. 7) is valid, and this method is implemented in the 1DHEAT code. Data from thin-film gages on Upilex are analyzed by the finite-volume method so no correction factors are required.

ADDITIONAL MATERIALS

Users wishing to incorporate new materials into the 1DHEAT code or modify current data must supply curve fit coefficients for the thermal conductivity, thermal diffusivity, thermal product and thermal product correction factors. These additions must be made in the "matprops" subroutine, and the choices must be added to the menu in the "readsetup" subroutine

The thermal diffusivity and thermal conductivity values for a material are defined in 1DHEAT by fourth-order polynomial curve fits (for lower-order curve fits, elements of the coefficient arrays may be set zero).

Thermal conductivity:

$$k(T) = a_1^{(k)} + a_2^{(k)} \cdot T + a_3^{(k)} \cdot T^2 + a_4^{(k)} \cdot T^3 \tag{C-13}$$

Thermal diffusivity:

$$\alpha(T) = a_1^{(\alpha)} + a_2^{(\alpha)} \cdot T + a_3^{(\alpha)} \cdot T^2 + a_4^{(\alpha)} \cdot T^3 \tag{C-14}$$

The thermal product and correction factor are defined by a three element array, β_i, where β_1, is the room temperature value of the thermal product, and the two remaining elements are the coefficients of a curve fit for the correction factor

$$\beta' = \beta_2 + \beta_3 (T - T_{amb}) \tag{C-5}$$

For metallic substrates that are represented by the variable thermal conductivity model, the first element is again the room temperature value of the thermal product, and the second and third elements are the coefficients for a thermal conductivity curve fit:

$$\frac{k}{k_0} = \beta_2 + \beta_3 \cdot T \tag{C-6}$$

VALIDATION OF THERMAL PROPERTIES DATA

As mentioned previously, the thermal properties data given in this work are in some cases quite different from data presented elsewhere. These differences are most pronounced for the materials Macor and quartz. Use of the current properties is validated by the results presented in Figure 32. This figure show the Stanton number distributions on two 1" radius hemisphere models tested side-by-side in the NASA LaRC 31" Mach 10 Air Tunnel.

One hemisphere was machined from quartz and one from Macor, and both were instrumented with thin-film resistance gages. These distributions are compared to a numerical solution computed using the viscous shock layer technique (courtesy of Roop Gupta at NASA Langley) and all distributions are normalized by the computed Fay-Riddell (ref. 27) stagnation point Stanton number. Both the quartz and Macor results obtained using the current values are within 5% of the computed VSL solution. It was found that experimental results computed using thermal property data from other references varied between 10% to 20% from the VSL solution.

APPENDIX D. 1DHEAT INPUT FILES

SETUP FILE "1Ddemocoax.inp"

Listing of sample setup file "1Ddemocoax.inp"

```
Sample Coaxial Thermocouple Hemisphere Data
300.2d0              ambient temperature (deg K)
1419.7d0             freestream velocity (m/s)
4.3078d-3            freestream density (kg/m3)
0.7603d6             total enthalpy (h_tot - h_298) (J/kg)
300.00d0             reference temperature (deg K)
Air                  test gas (Air, He, N2, CF4, CO2)
2.5d0                time zero (sec)
0.02d0               data sampling period (sec)
300                  number of points in integration window
4.0d0                start time of averaging window (sec)
4.5d0                end time of averaging window (sec)
1.0d0                adiabatic wall recovery factor
2                    columns of position data
S/R                  title of position column #1
theta                title of position column #2
GAGEID      S/R          theta        ALPHA_R      GAGE TYPE    SUBSTRATE
'TC7'       -1.5709      -90.0        0.00         coax         chromel
'TC6'       -1.3091      -75.0        0.00         coax         chromel
'TC5'       -1.0472      -60.0        0.00         coax         chromel
'TC4'       -0.7854      -45.0        0.00         coax         chromel
'TC3'       -0.5236      -30.0        0.00         coax         chromel
'TC2'       -0.2618      -15.0        0.00         coax         chromel
'TC1'       -0.0000        0.0        0.00         coax         chromel
end
```

Description of "1Ddemocoax.inp" file

Line 1:		Text header describing the data.
Line 2:	T_{amb}	Ambient temperature before the run
Line 3:	u_∞	freestream velocity
Line 4:	ρ_∞	freestream density
Line 5:	Δh_{tot}	total enthalpy, $\Delta h_{tot} = h(T_{tot}) - h(T_{rp})$
Line 6:	T_{ref}	reference temperature at which to extrapolate heating rates
Line 7:	gas	identifies test gas. Must be "Air", He", "N2", "CF4" or "CO2".
Line 8:	t_0	time zero. Time at which data reduction begins
Line 9:	Δt	time between data samples.
Line 10:	n_{tot}	number of data points after time zero to continue data reduction
Line 11:	t_1	start time of window over which reduced data is to be averaged
Line 12:	t_2	end time of window over which reduced data is to be averaged

Line 13:	r	adiabatic wall recovery factor used in Stanton number calculation
Line 14:	n_{col}	number of columns (maximum of 4) of position data to be read
Lines 15 -16:		titles of position data columns.
Line 17:		Text header identifying data in following lines.
Line 18-24:	Gage data lines which contain:	
	gageid(n):	identifier for *nth* gage, may be up to 6 characters
	pos(n,k):	numerical position data for *nth* gage corresponding to *kth* position column data title
	α_R (n)	temperature coefficient of resistance (in 1/°R) for the *nth* thin-film gage. This is a dummy value for coaxial thermocouples or if the raw data is already converted to °K
	gage type	either "coax" (for coaxial thermocouple) or "thinfilm" (for thin-film gage)
	substrate	substrate material. For multi-layer substrates, this identifies the material properties to be used to reduce the data if the analytical method is chosen and the substrate is approximated as a single layer

Line 25 Terminates reading of gage data

The flow properties information in the setup file is not required for the computation of the heat transfer rates. However, it is used in the computation of the Stanton number, C_h, the heat transfer coefficient, H, and the reference heating value, q_{ref}. It must be emphasized that the heat transfer coefficient computations are only as accurate as the user-input flow properties information. Furthermore, one of the inherent assumptions in these computations is that the flow is steady; that is, the density, velocity and total enthalpy do not vary with time. For unsteady flow, these results will not be valid.

Wall enthalpy as a function of temperature is also required for the heat transfer coefficient computations. Currently, 1DHEAT incorporates enthalpy curve fits for air, N_2, He, CF_4 and CO_2 gases. The curve fit coefficients are taken from McBride (ref. 28), and are valid for wall temperatures between 300°K and 1000°K. If needed, additional curve fits may be added in the "hwall" function of the code, and the additional choices can be added to the menus in the "readsetup" subroutine.

Several times are required in the input file. The times t_1 and t_2 define the start and end of the window over which the data is to be averaged. Initial selection of the proper averaging window in the input file is not critical, as the data can easily be re-averaged using 1DHEAT code options 3 or 7. In fact, a better definition of the averaging window can be made by first running the code with assumed window start and end times, and then analyzing the heat transfer-time histories to determine the optimum values for t_1 and t_2.

The time t_0 defines the point at which reduction of the data begins. The exact definition of t_0 is also not critical as long as t_0 is before the gages experiences any heating. In fact, there is a built-in safety factor on t_0 in this

code that will step back 50 time increments from the user-input value (or fewer if there are less than 50 data points) Note that the 1DHEAT code will compute baseline pre-test voltages (for thin-film gages) for each sensor by averaging over the first 25 points from t_0. The 50-point safety factor and 25-point baseline averaging values are set in the 'setup' subroutine of the code.

Entries in the input file must correspond to allowable values. Allowable text strings for the test gas are "Air", "N2", "CF4" "He" and "CO2". The gage type can be "thinfilm" for thin-film resistance gages or "coax" for coaxial surface thermocouples. Finally, the substrate type can be set to "macor", "quartz", "pyrex", "chromel", "constantan", "stainless", or "upilex".

FINITE-VOLUME SETUP FILE "1Ddemocoax.fvinp"

Listing of sample setup file "1Ddemocoax.fvinp"

```
SAMPLE COAX DATA FINITE-VOLUME SETUP FILE
GAGEID      LAYERS      WALL BC
Layer #     NODES       THICKNESS          SUBSTRATE
'TC7'       1           0
 1          43          1.27d-2            chromel
'TC6'       1           0
 1          43          1.27d-2            chromel
'TC5'       1           0
 1          43          1.27d-2            chromel
'TC4'       1           0
 1          43          1.27d-2            chromel
'TC3'       1           0
 1          43          1.27d-2            chromel
'TC2'       1           0
 1          43          1.27d-2            chromel
'TC1'       1           0
 1          43          1.27d-2            chromel
end
```

Description of "1Ddemocoax.fvinp" file

Line 1: Text header describing the file

Line 2: Column titles

Line 3: Column titles continued

Lines (4,5), (6,7), etc.:

The first line in each pair contains

gageid(n): identifier for *nth* gage, may be up to 6 characters

nlay(n): number of substrate layers of *nth* gage

nbc(n): interior boundary condition for *nth* gage
(0 for adiabatic, 1 for constant ambient temperature)

The second line in each pair contains

k:	layer number
nplay(n,k):	number of points in *kth* layer of *nth* gage
d(n,k):	thickness of *kth* layer of *nth* gage
subs(n,k):	substrate material of *kth* layer of *nth* gage

Note that in this example, the substrate has only one layer. A substrate with more layers would have additional lines of the same form as line 5. For example a thin-film gage on a 2 mil (0.0508 mm) layer of Upilex over a 1/4" (0.635 cm) thick Macor layer with 5 nodes in the upilex layer and 244 nodes in the Macor layer would have lines of the following form for each gage:

```
'TF1'       2           0
 1          5           5.08d-5          upilex
 2          244         6.35d-3          macor
```

INPUT TEMPERATURE FILE "1Ddemocoax.degk"

Listing of sample input file "1Ddemocoax.degk"

```
1  Time     TC7      TC6      TC5      TC4      TC3      TC2      TC1
2  0.0000   300.25   300.19   300.23   300.21   300.21   300.23   300.22
3  0.0200   300.24   300.19   300.24   300.19   300.21   300.23   300.22
4  0.0400   300.21   300.18   300.21   300.18   300.19   300.21   300.21
5  ... (remainder of file omitted)
```

Description of "1Ddemocoax.degk" file

Line 1:	Text header describing following lines.
Lines 2+:	Contain the time index followed by the temperatures (or voltages in a ".volt" file) for each gage at that time index. Reading is terminated by the end of the file

Note that a voltage input file (with a '.volt' extension) will have the same format except that temperatures are replaced with voltages.

TABLE 1. 1DHEAT data files

File template: 1D**testIDrunID**.*ext*

Extension		Description
.inp	-	setup file
.fvinp	-	finite-volume setup data
.volt	-	raw data (volts)
.degk	-	raw data (°K)
.t	-	time history of sensor temperatures
.qx	-	time history of heat transfer
.chx	-	time history of Stanton number
.qresx	-	time history of heat transfer residual
.chresx	-	time history of Stanton number residual
.distx	-	time-averaged heat transfer data
.distxnew	-	recomputed time-averaged heat transfer data
.tback	-	back face temperature-time histories
.gageid	-	temperature profile though substrate of sensor "gageid"

x is the data reduction method:
1) indirect semi-infinite
2) direct semi-infinite
3) finite-volume

TABLE 2. Thermocouple Coefficients from National Bureau of Standards

	Type-E Thermocouple
a_0	0.104967248
a_1	17189.45282
a_2	-282639.0850
a_3	12695339.5
a_4	-448703084.6
a_5	1.10886×10^{10}
a_6	-1.76807×10^{11}
a_7	1.71842×10^{12}
a_8	-9.19278×10^{12}
a_9	2.06132×10^{13}

TABLE 3. 31" Mach 10 Air Flow Conditions

	"demothin"	"democoax"
p_1 (Pa)	65.18	70.11
T_1 (°K)	52.73	53.04
u_1 (m/s)	1419	1413
M_1	9.75	9.68
Re_1 (1/m)	1.570×10^6	1.661×10^6
$p_{0,2}$ (Pa)	8048.8	8528.0
$T_{0,2}$ (°K)	1012.0	1004.2
$\Delta h_{0,2}$ (J/kg)	0.760×10^6	0.751×10^6

TABLE 4. Approximate room temperature material properties

MATERIAL	ρ (kg/m^3)	c_p (J/kg-°K)	k (W/m-°K)	α (m^2/s)	β (W-s$^{1/2}$/m^2-°K)
CHROMEL	8714	458	17.5	4.40×10^{-6}	8376
CONSTANTAN	8906	395	22.4	6.34×10^{-6}	8840
MACOR	2568	731	1.46	7.94×10^{-7}	1642
QUARTZ	2192	726	1.30	8.15×10^{-7}	1435
PYREX	2227	458	1.37	8.10×10^{-7}	1527
UPILEX	1490	967	0.303	2.11×10^{-7}	661
17-4 STAINLESS	7800	460	16.0	4.47×10^{-6}	7587

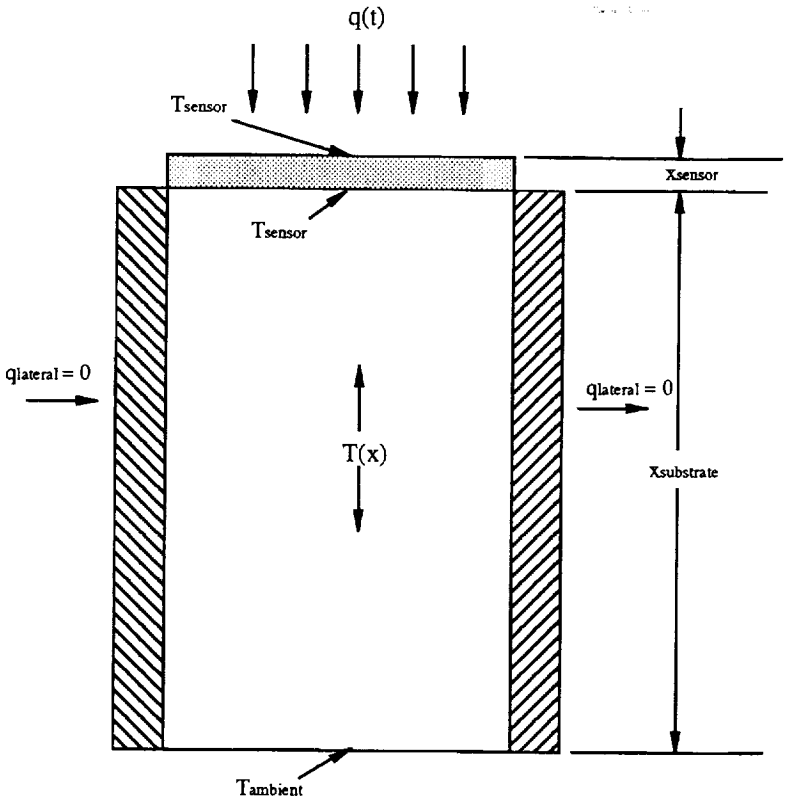


FIGURE 1: Generic temperature sensor and substrate

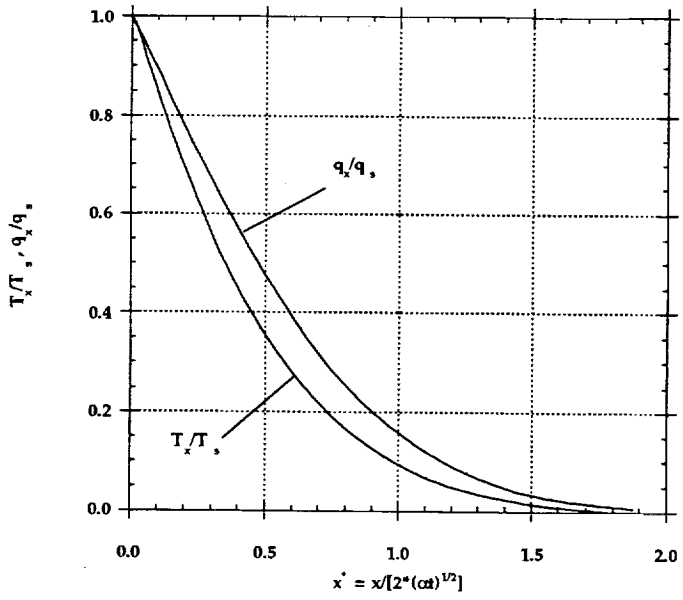


FIGURE 2: Semi-infinite test time for constant heat flux (redrawn from reference 2)

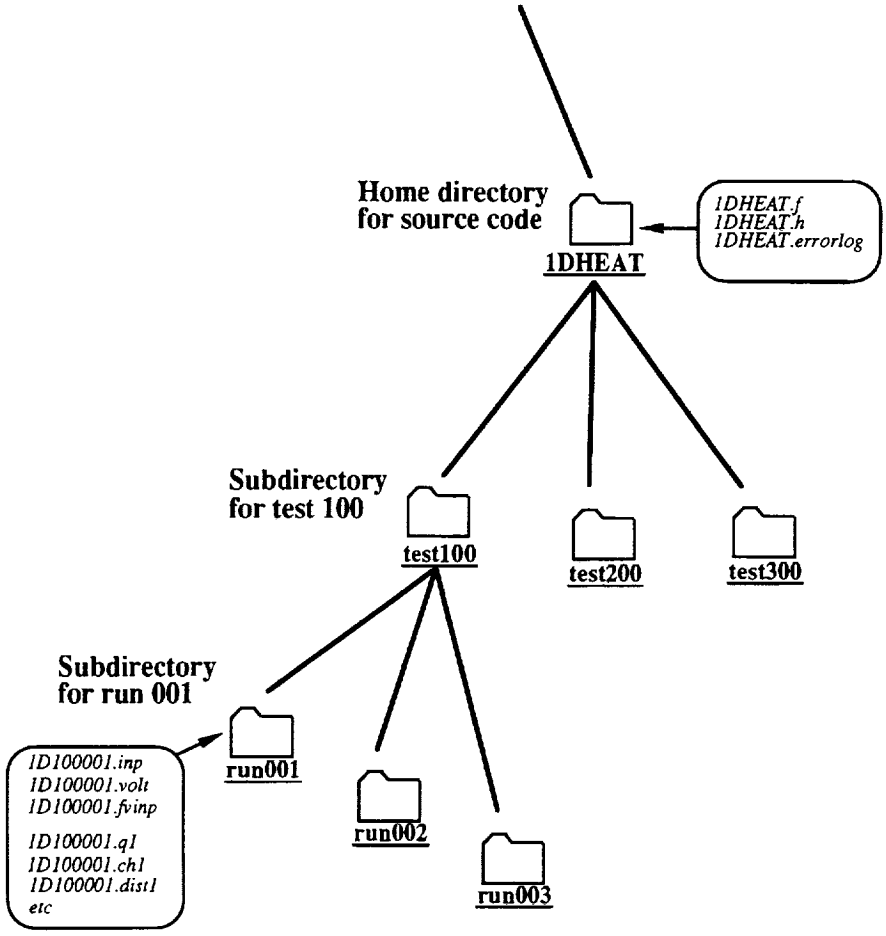


FIGURE 3: 1DHEAT directory structure

```
        "1DHEAT" v2.20 PROGRAM OPTIONS:

   SEMI-INFINITE METHOD
          1. Reduce raw data (volts).
          2. Reduce raw data (degrees K).
          3. Recompute statistics over new
             time interval.
          4. Compute residuals.

   FINITE-VOLUME METHOD
          5. Reduce raw data (volts).
          6. Reduce raw data (degrees K).
          7. Recompute statistics over new
             time interval.
          8. Compute residuals.
          9. Temperature profile for a gage at a
             specified time.

         10. Quit.
```

FIGURE 4: 1DHEAT main menu

FIGURE 5: Temperature-time histories for coaxial thermocouple data set

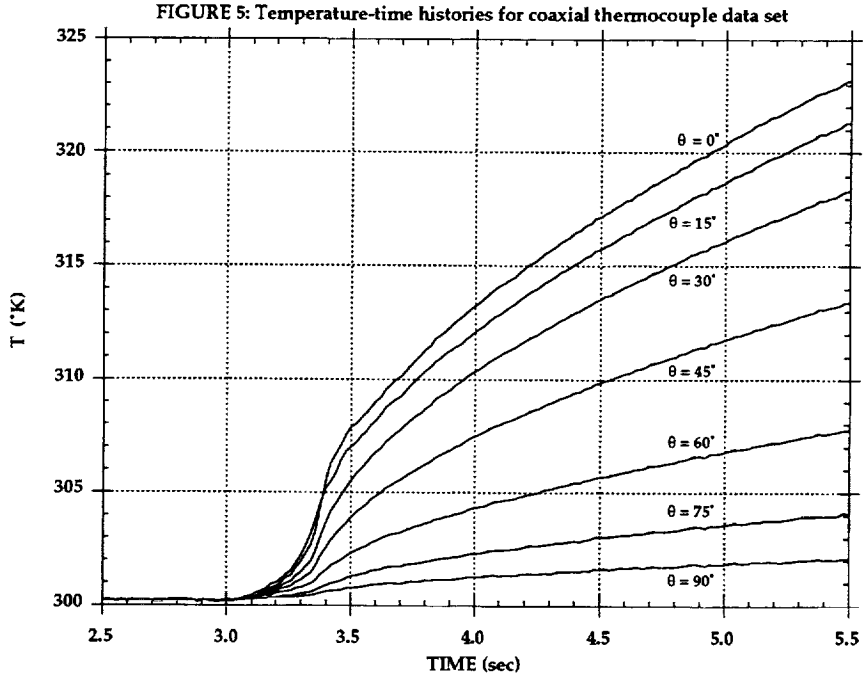


FIGURE 6: Stagnation point heating-time history for coaxial thermocouple data set

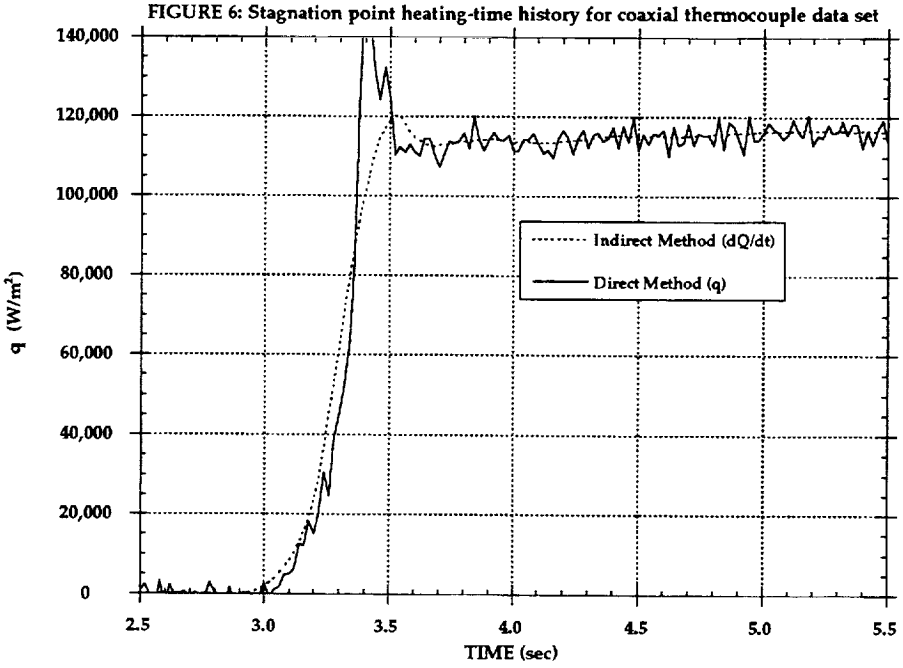


FIGURE 7: Stagnation point heat flux and Stanton number time histories for coaxial thermocouple data set

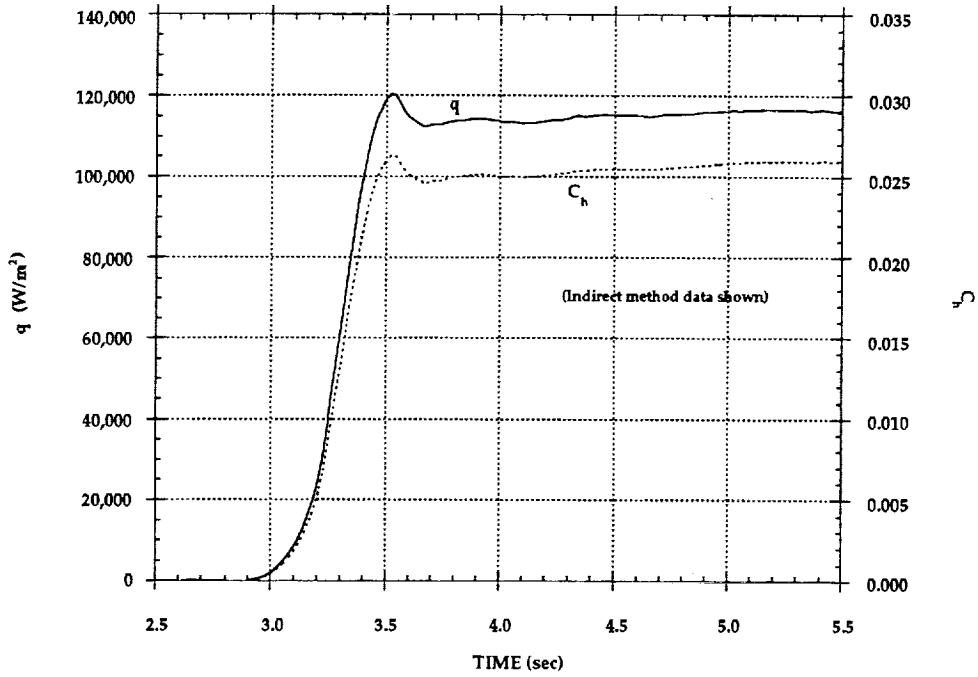


FIGURE 8: Averaged surface heat distributions for coaxial thermocouple data set

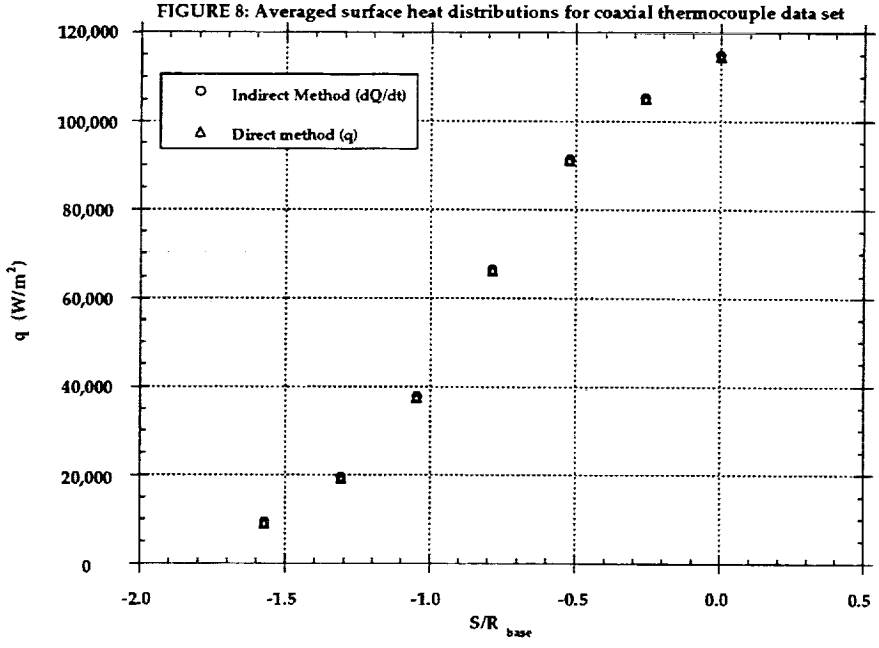


FIGURE 9: Heat flux surface distribution with standard deviations for coaxial thermocouple data set

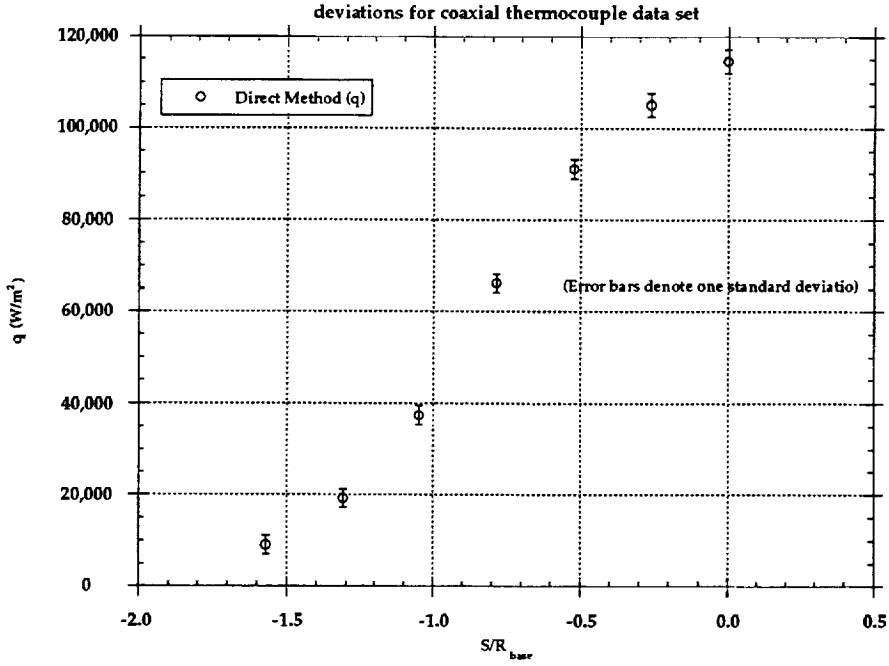


FIGURE 10: Temperature-time histories for thin-film gage data set

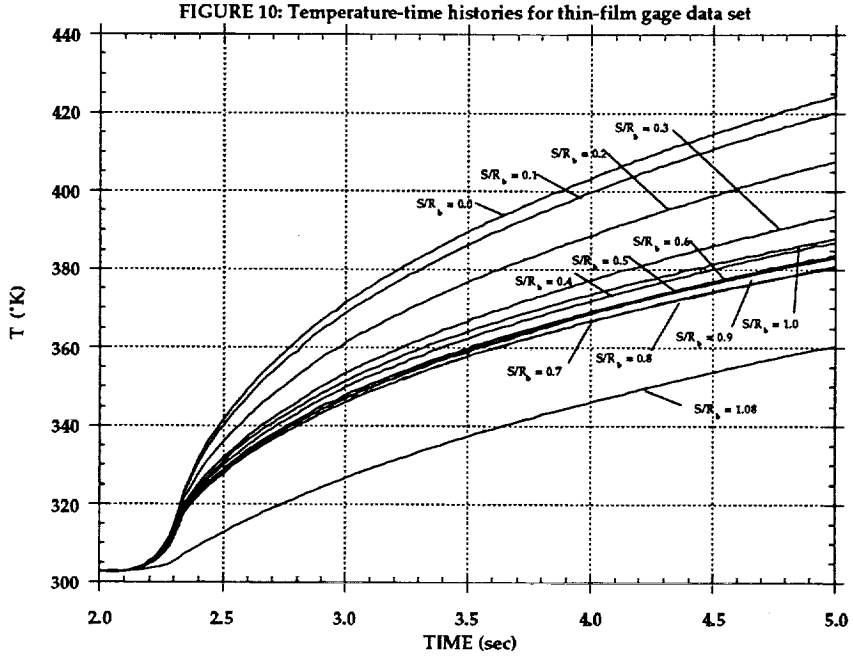


FIGURE 11: Stagnation point heating-time history for thin-film gage data set

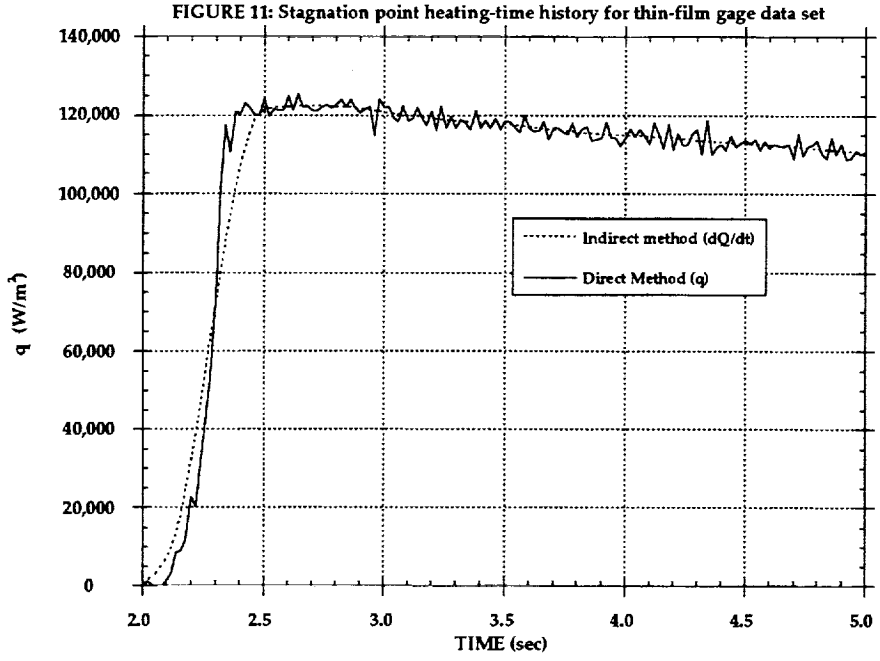


FIGURE 12: Stagnation point heat flux and Stanton number time histories for thin-film gage data set

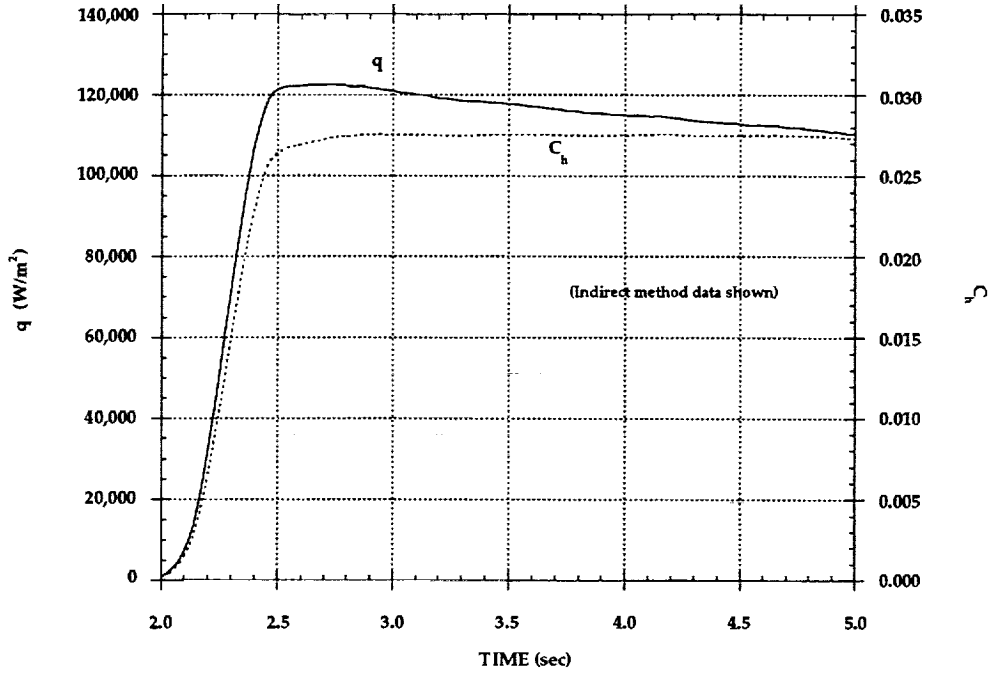


FIGURE 13: Averaged surface heat flux distributions for thin-film gage data set

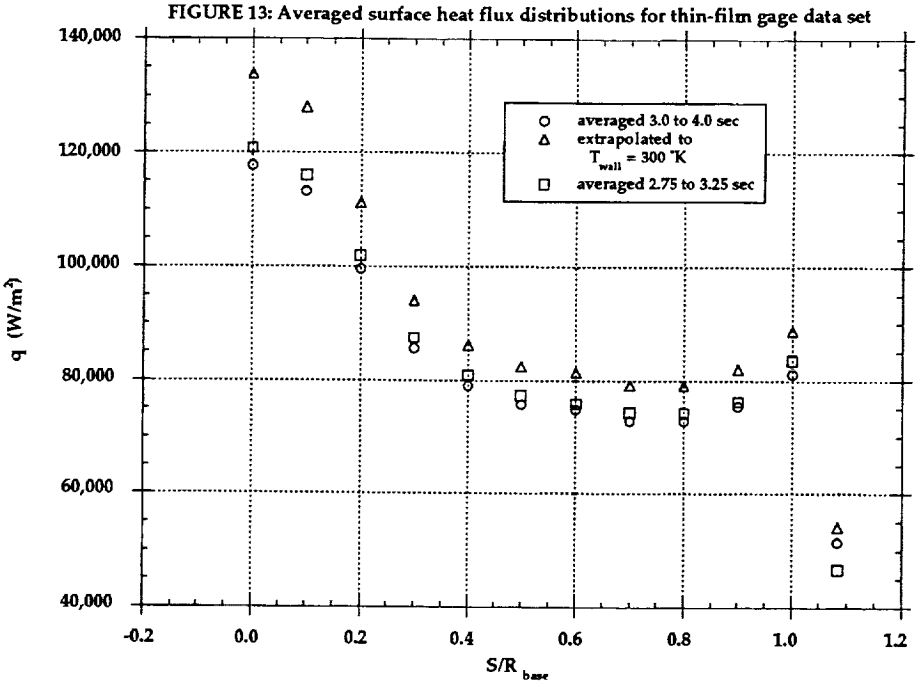


FIGURE 14: Averaged Stanton number distributions for thin-film gage data set

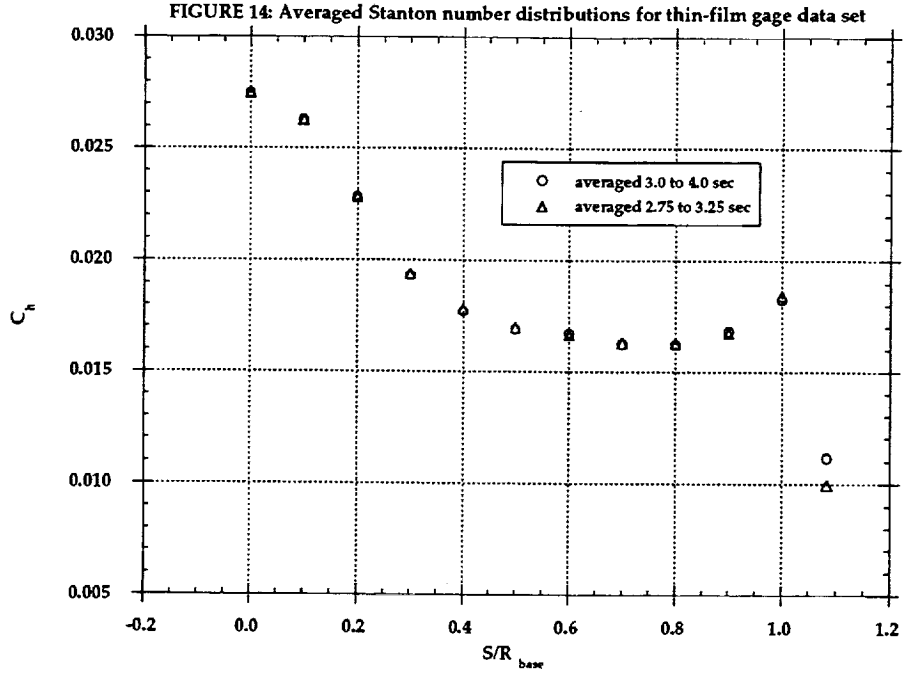


FIGURE 15: Stagnation point Stanton number-time history for thin-film gage data set

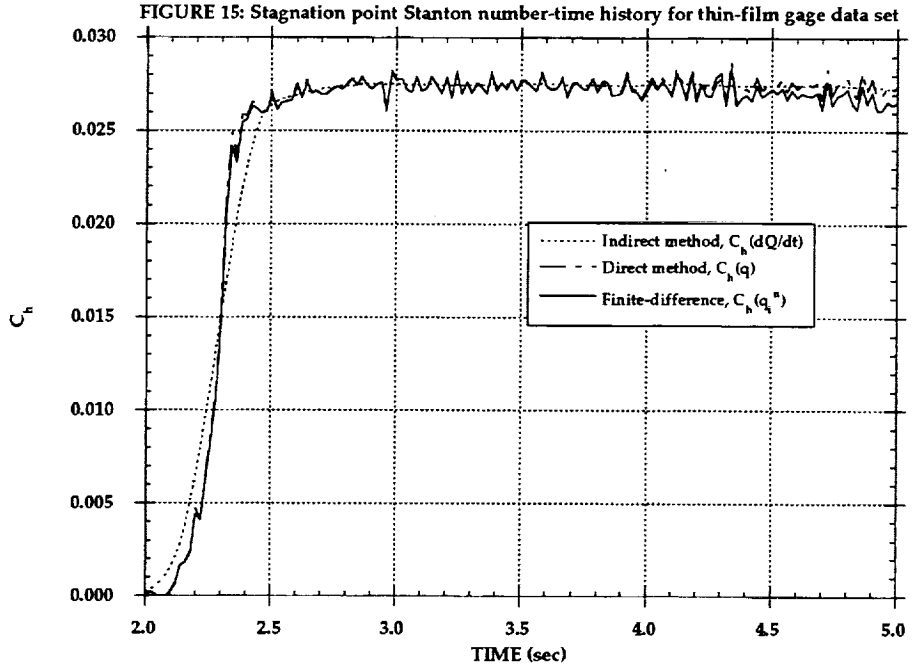


FIGURE 16: Temperature profiles through stagnation point gage substrate for thin-film gage data set

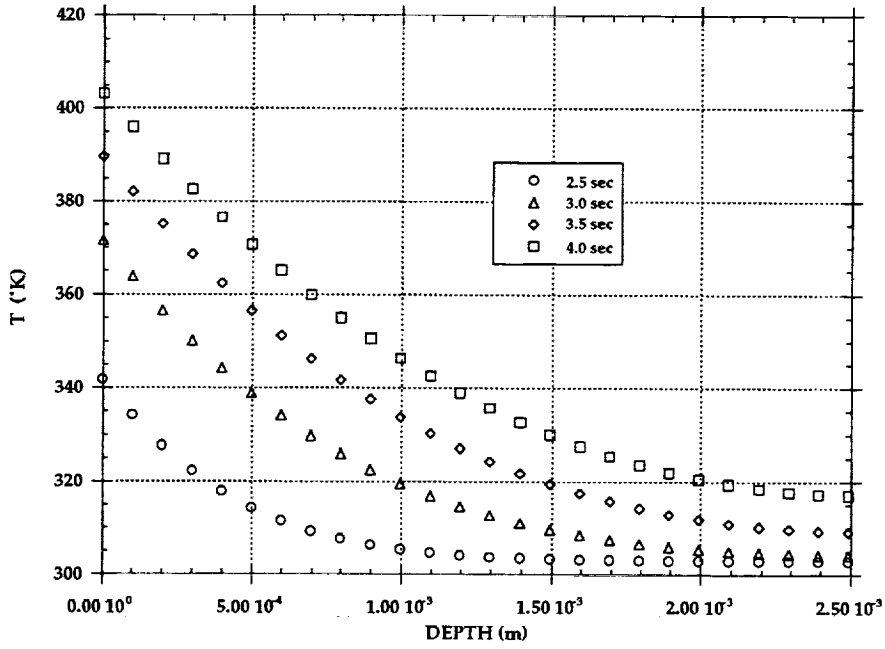


FIGURE 17: Back-face temperature-time histories for thin-film gage data set

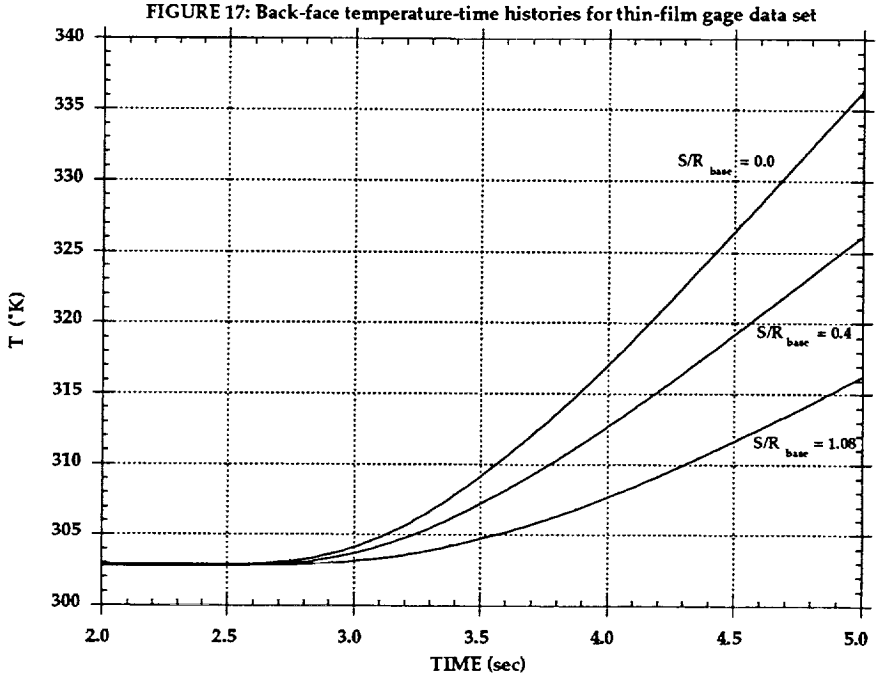


FIGURE 18: Normalized Stanton number distributions on 70° sphere-cones

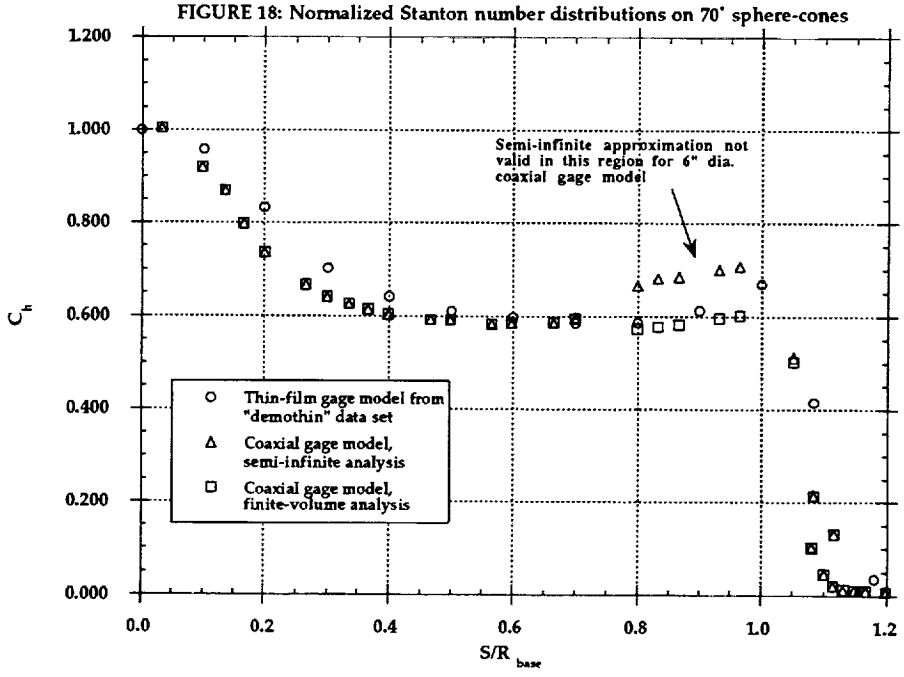


FIGURE 19: Heating distribution on 0.25" radius cylinder

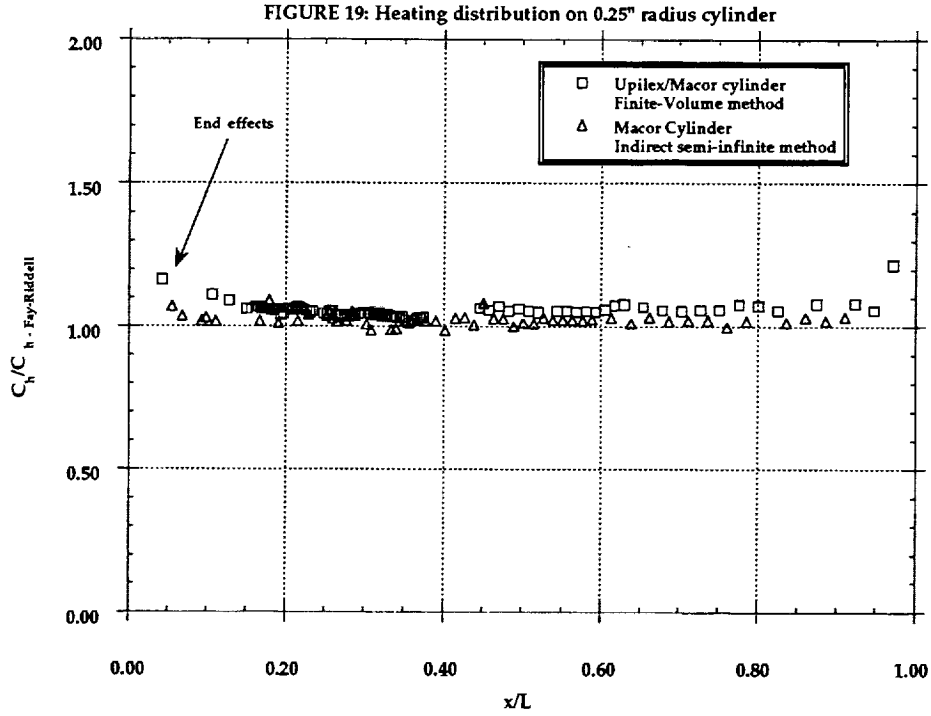
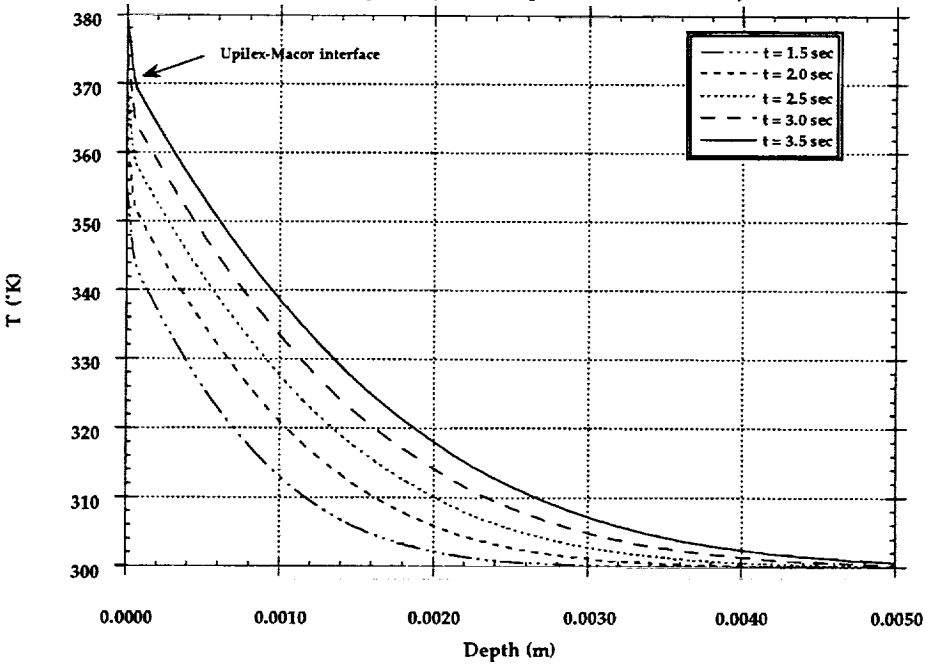


FIGURE 20: Temperature profile through substrate of 0.25" radius cylinder



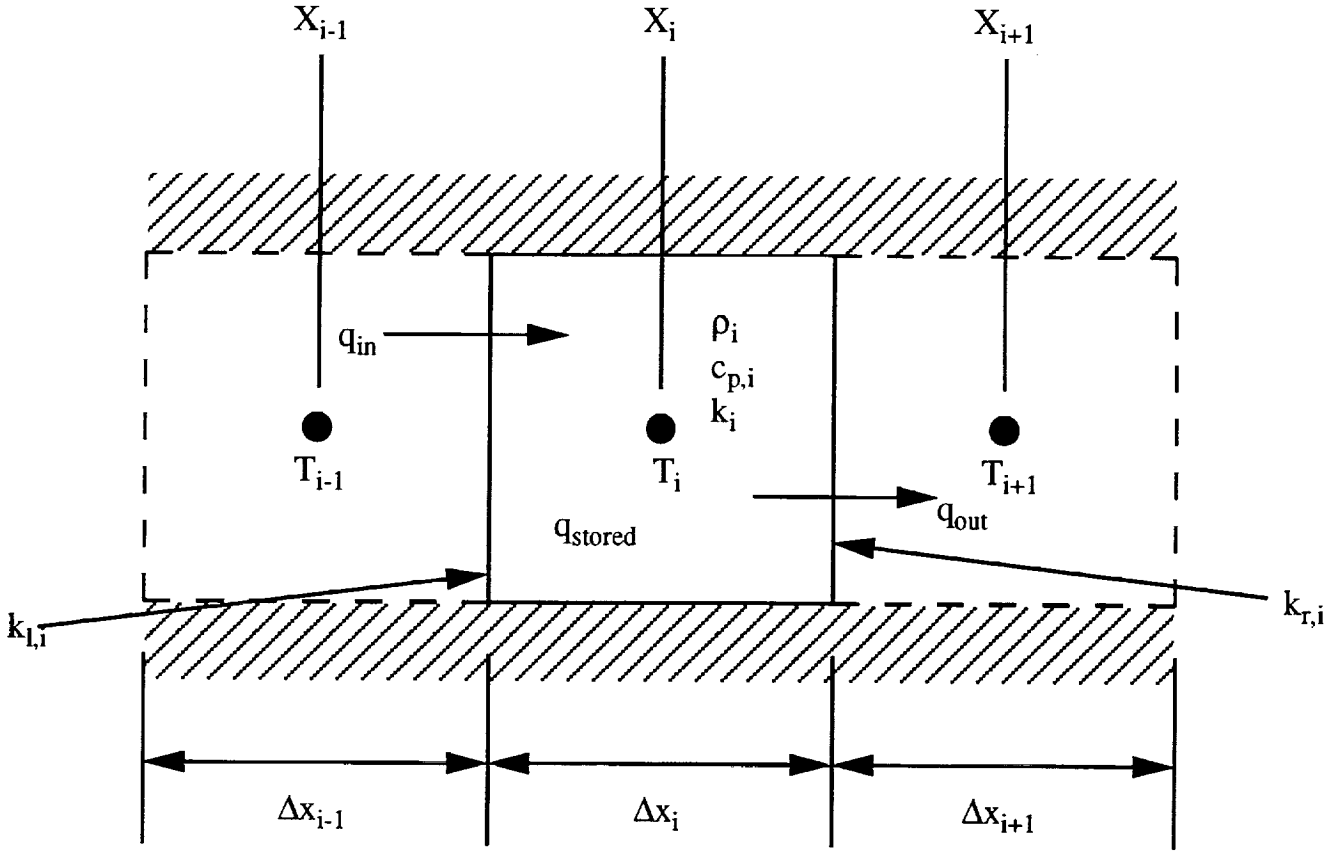


Figure 21: Notation for finite-volume method

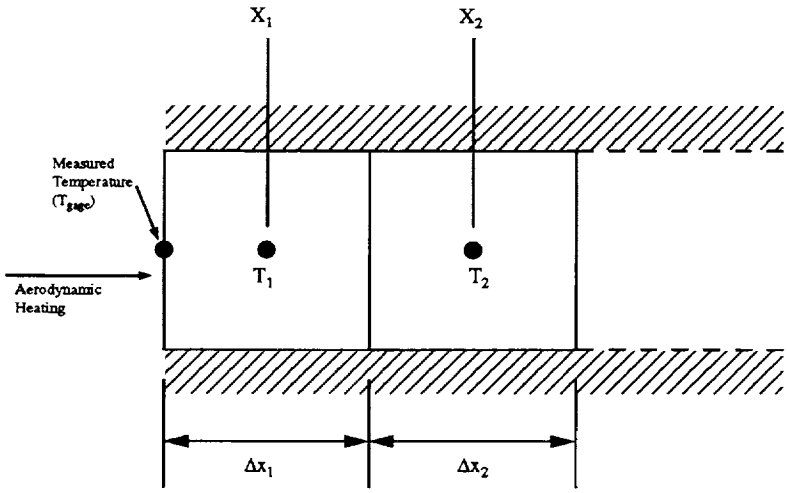
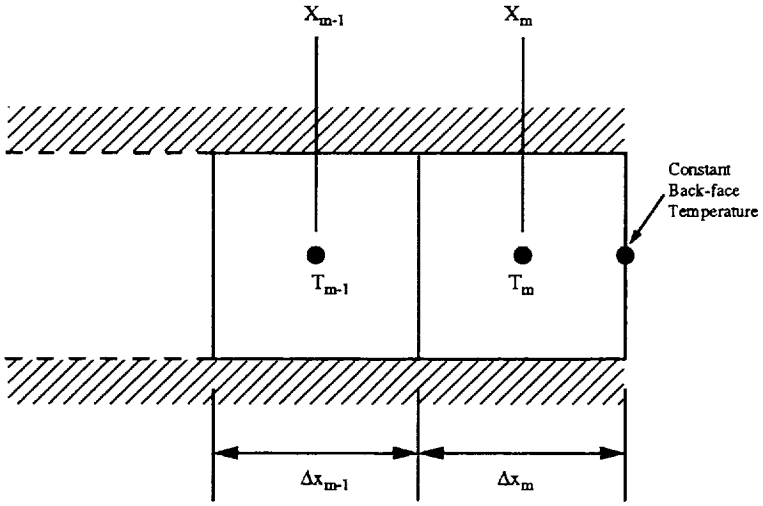


Figure 22a: Surface boundary condition



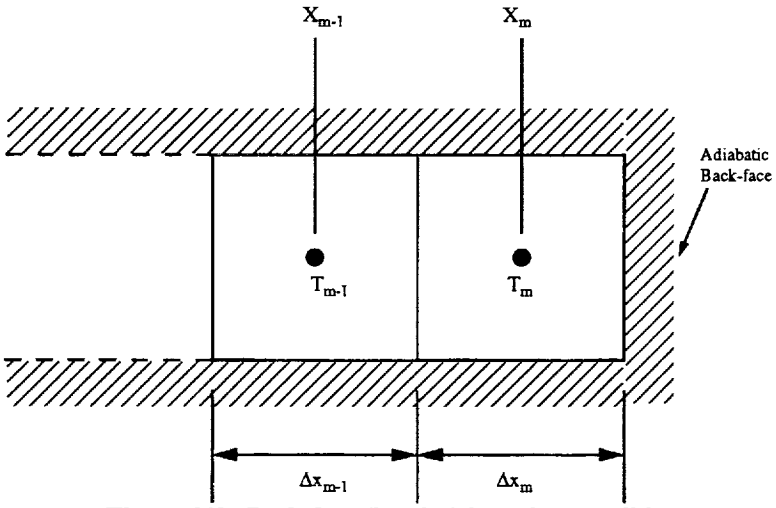


Figure 22b: Back-face (interior) boundary conditions

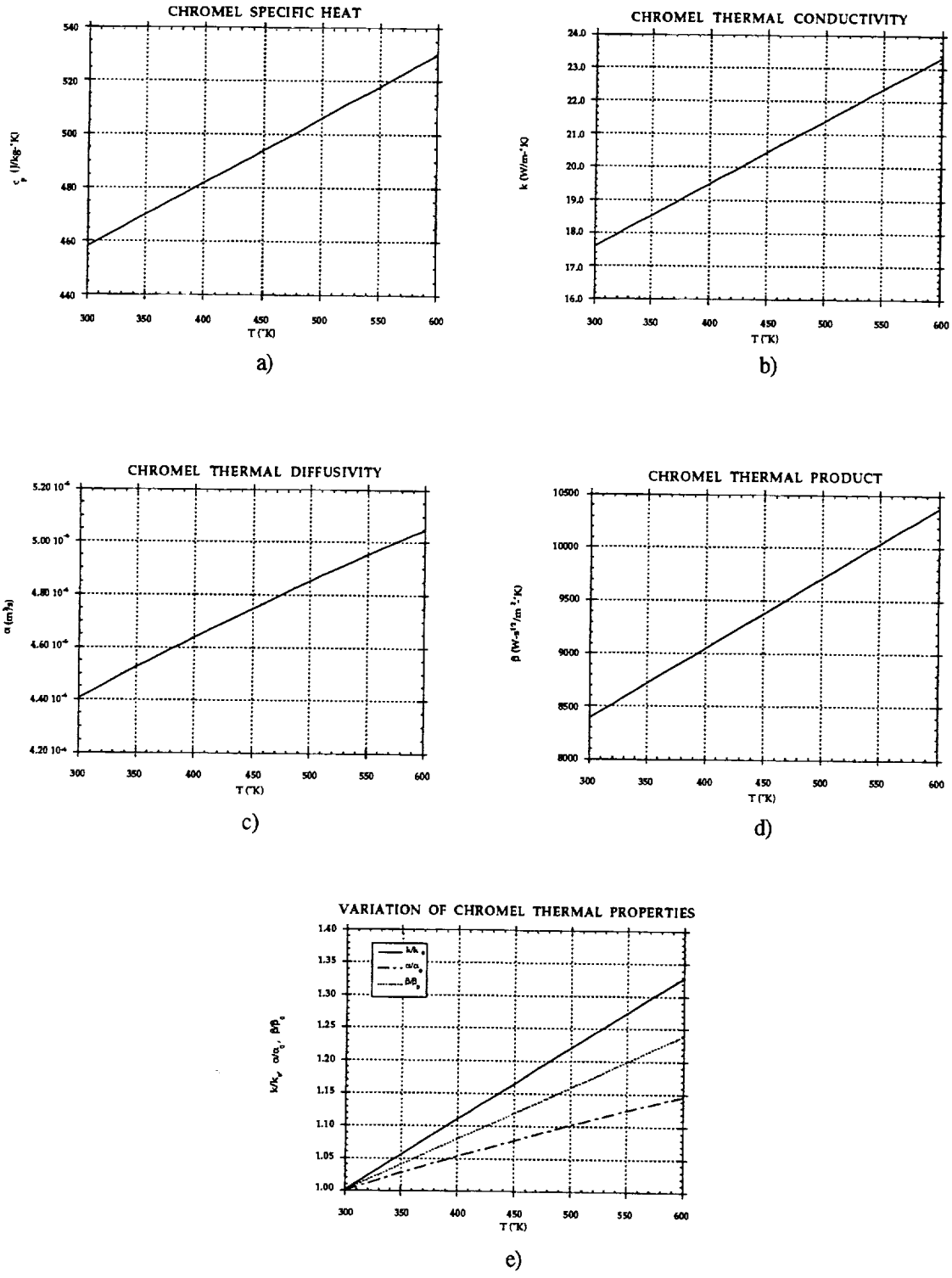
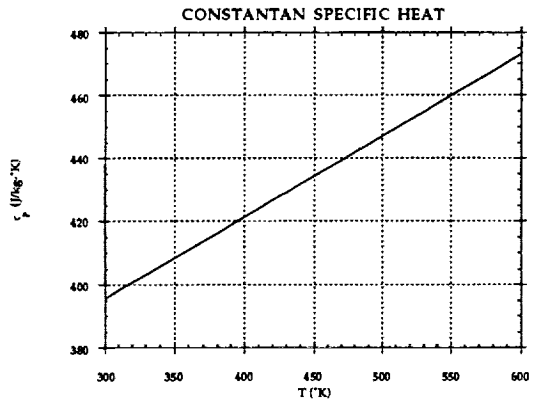
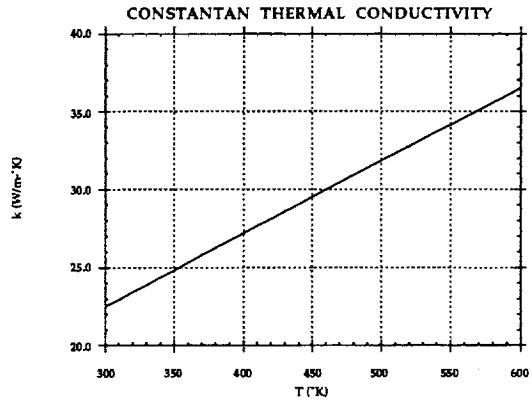


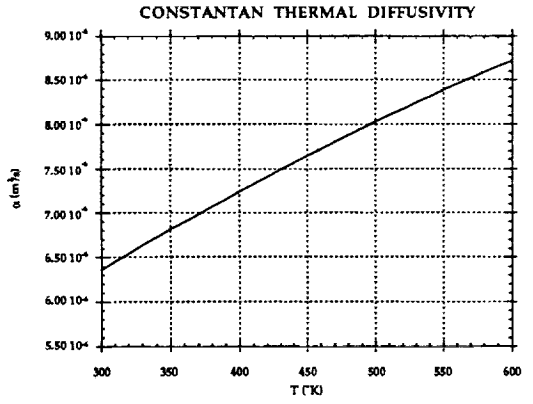
Figure 23: (a-e) Chromel thermal properties



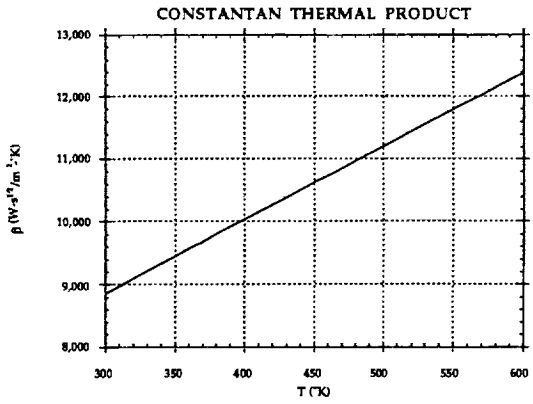
a)



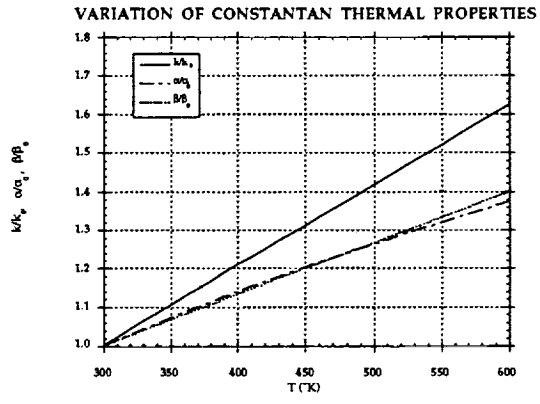
b)



c)



d)



e)

Figure 24: (a-e) Constantan thermal properties

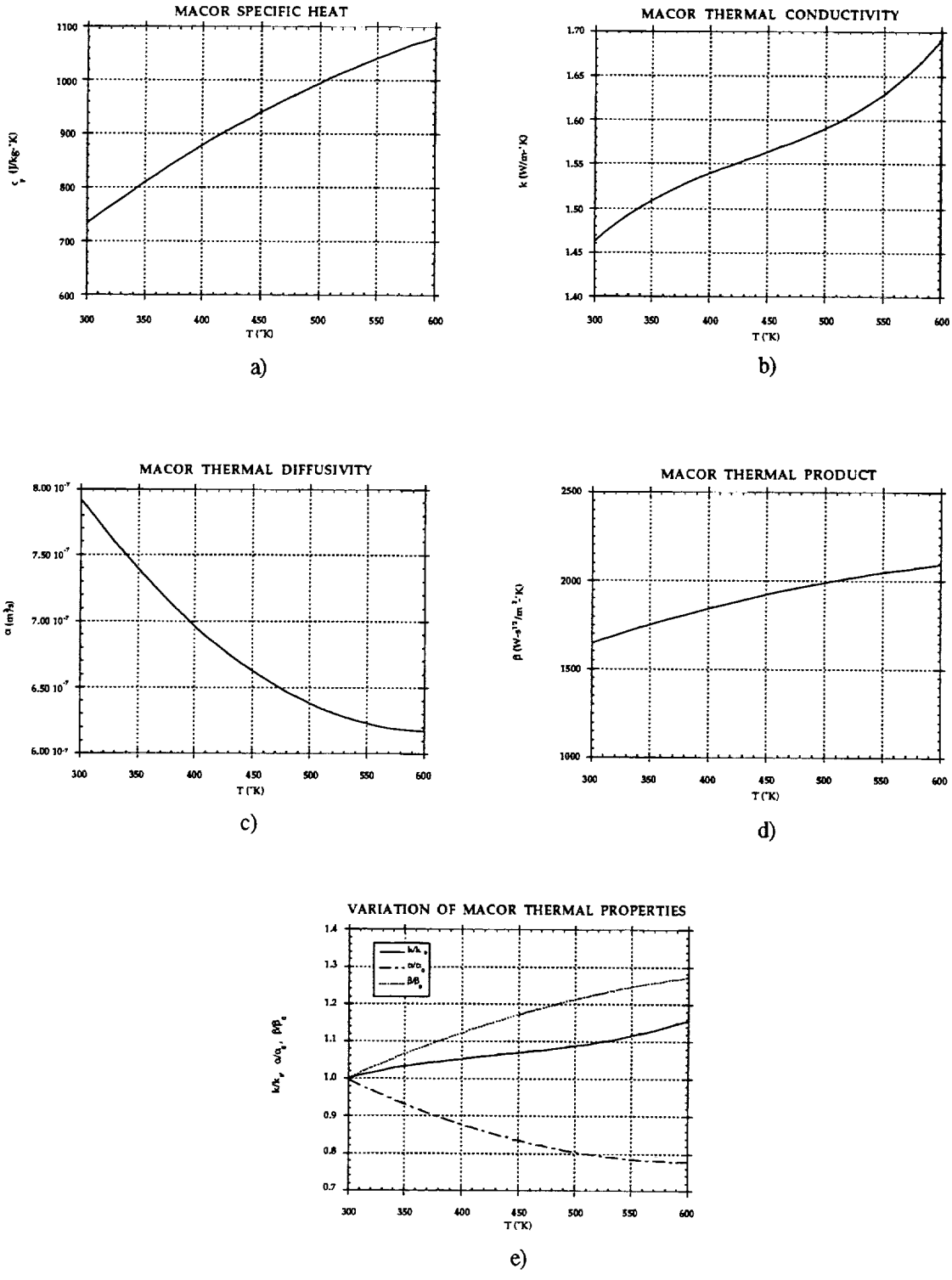


Figure 25: (a-e) Macor thermal properties

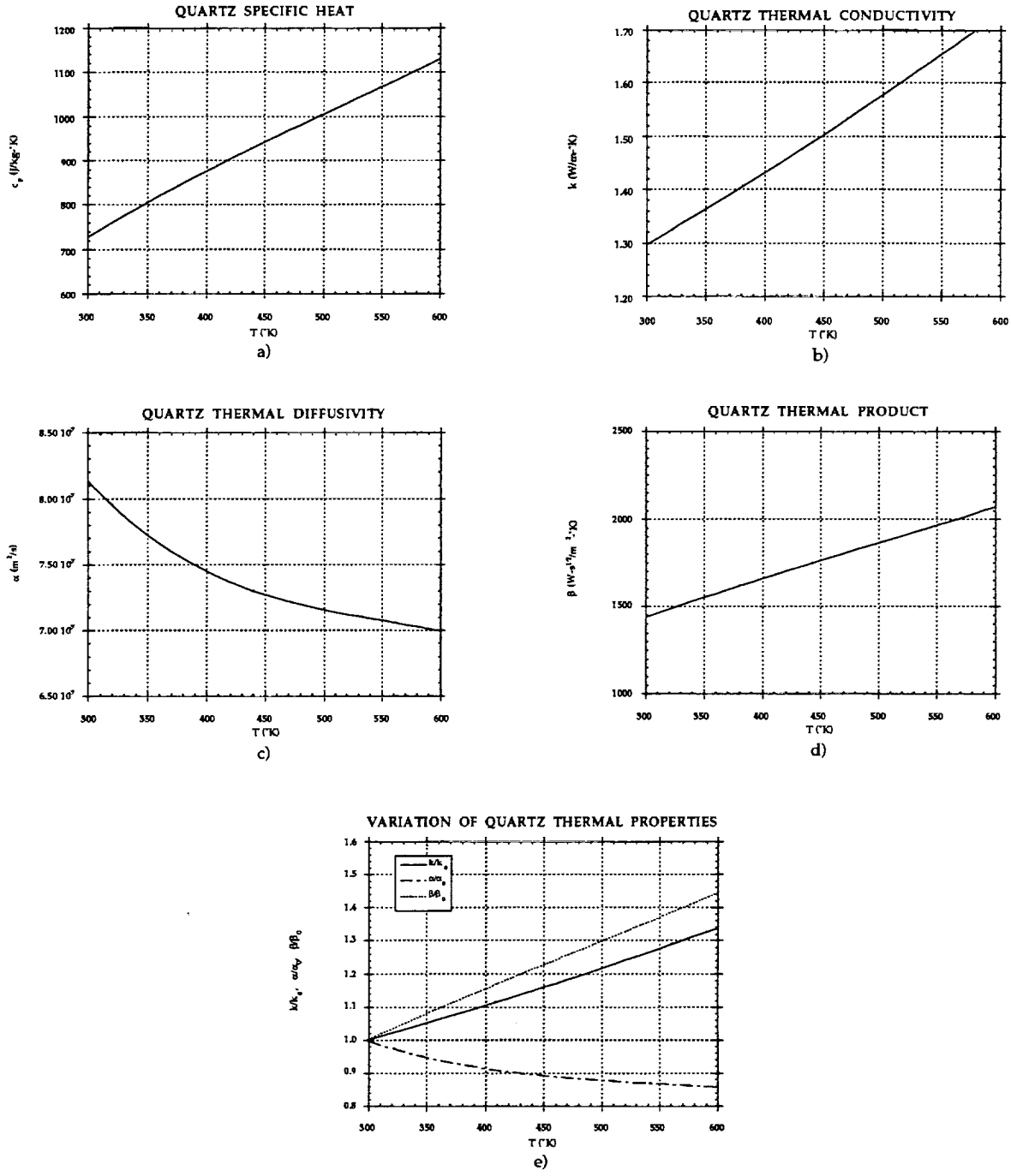


Figure 26: (a-e) Quartz thermal properties

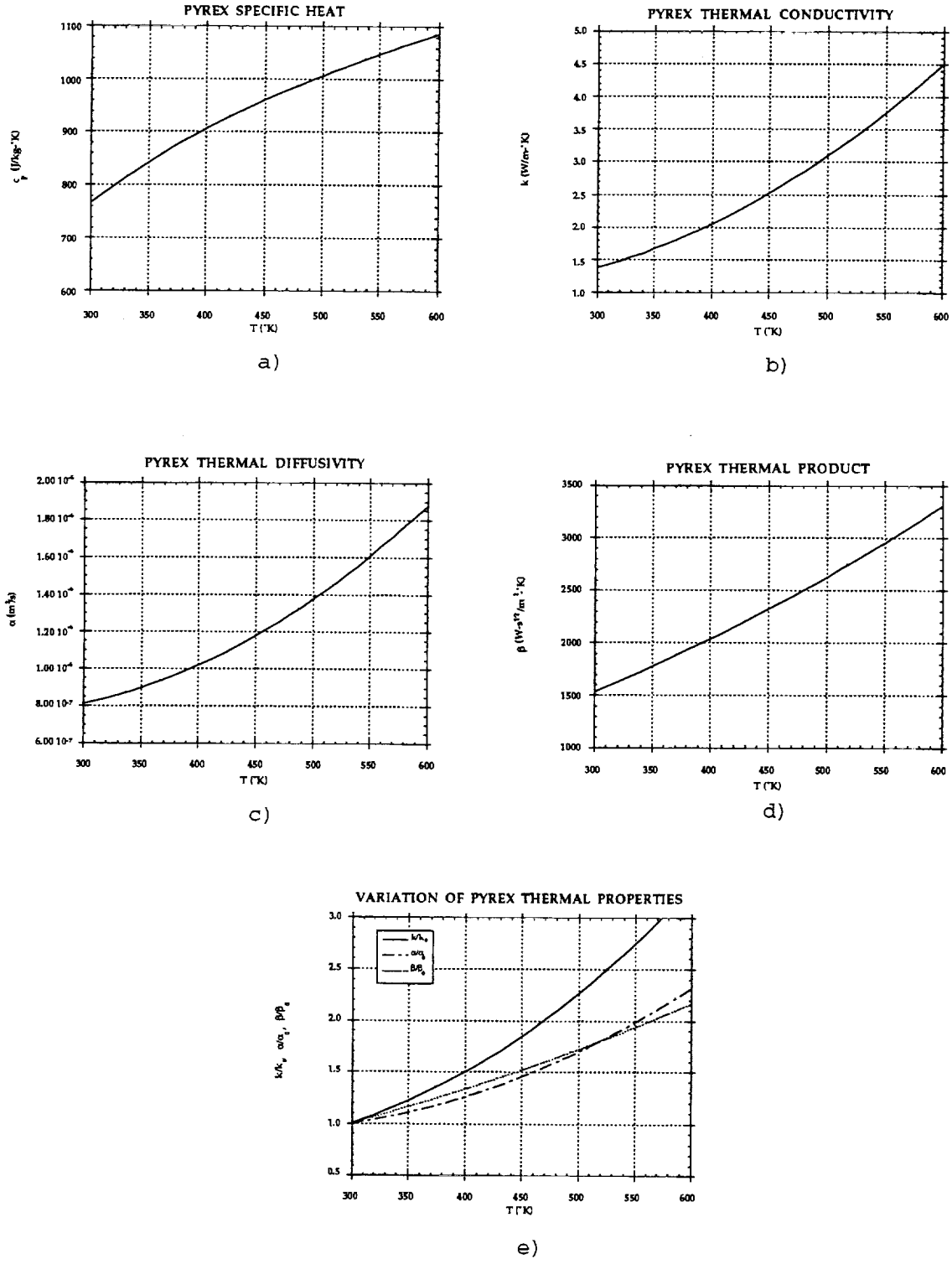


Figure 27: (a-e) Pyrex thermal properties

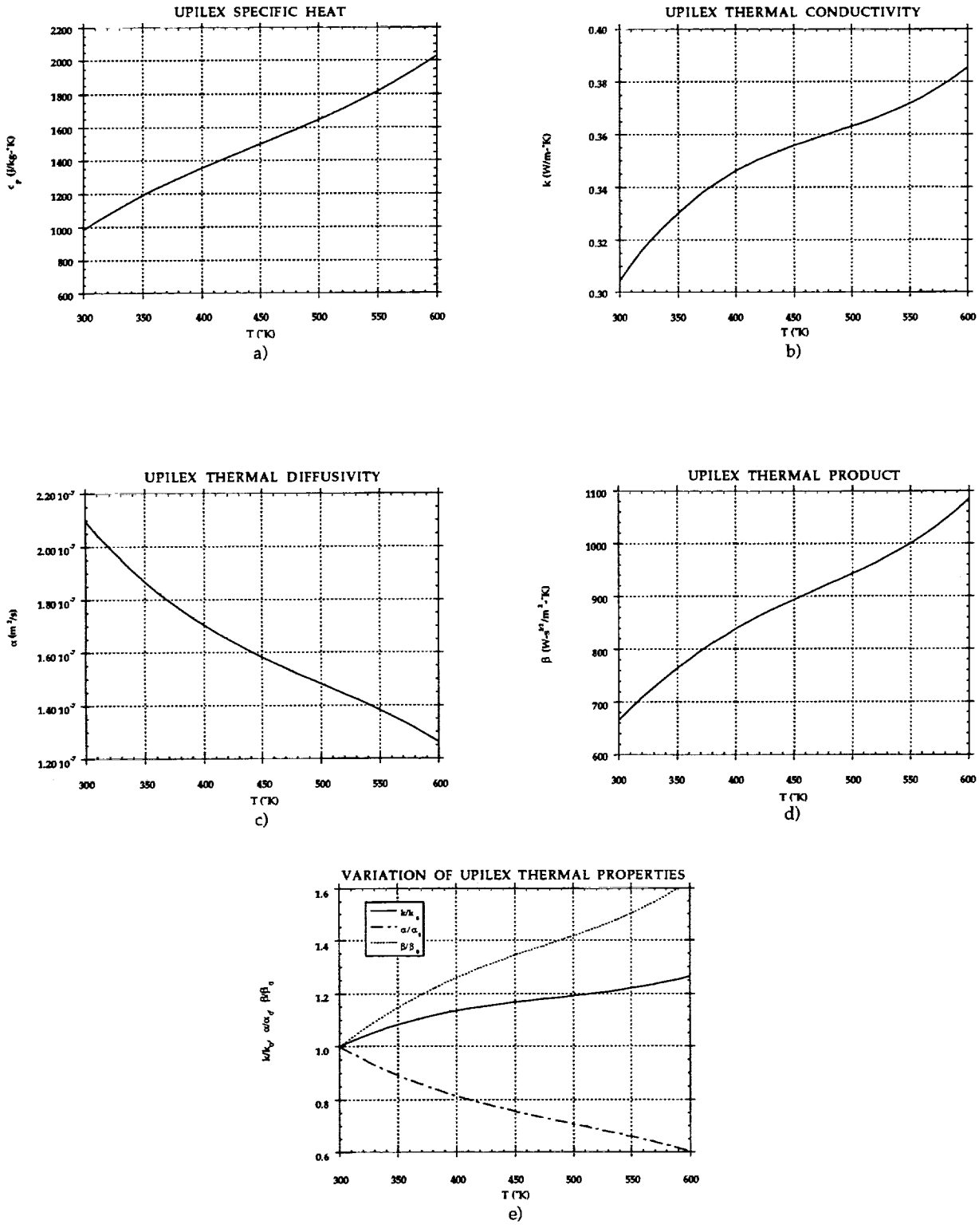


Figure 28: (a-e) Upilex thermal properties

FIGURE 29: Finite-volume solutions for constant and variable thermal properties test cases

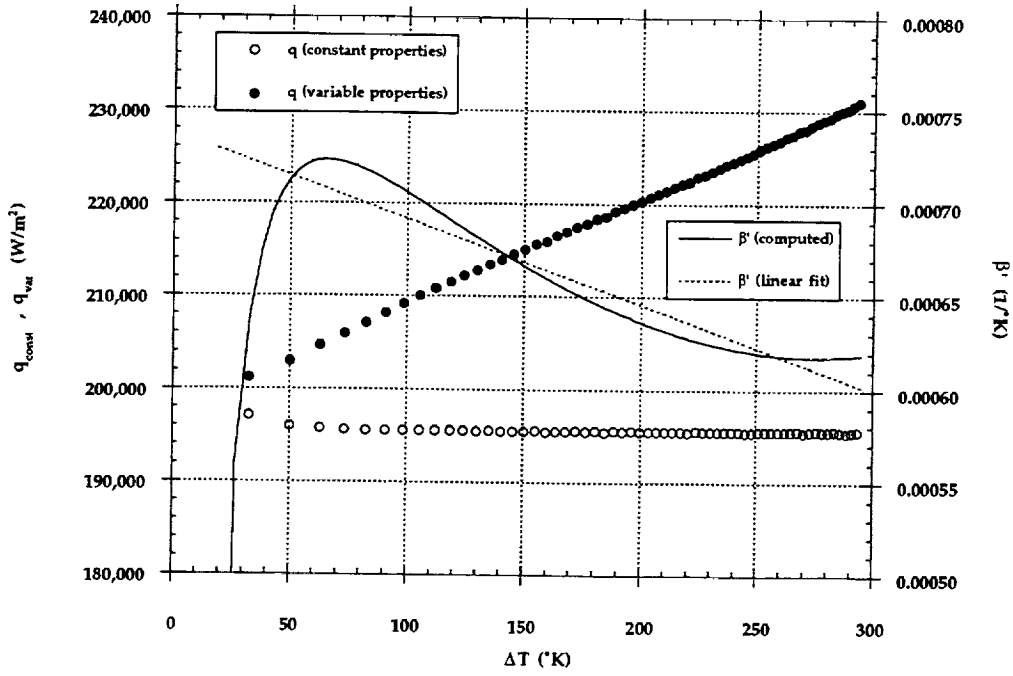


FIGURE 30: Finite-volume solution and corrected analytical solution

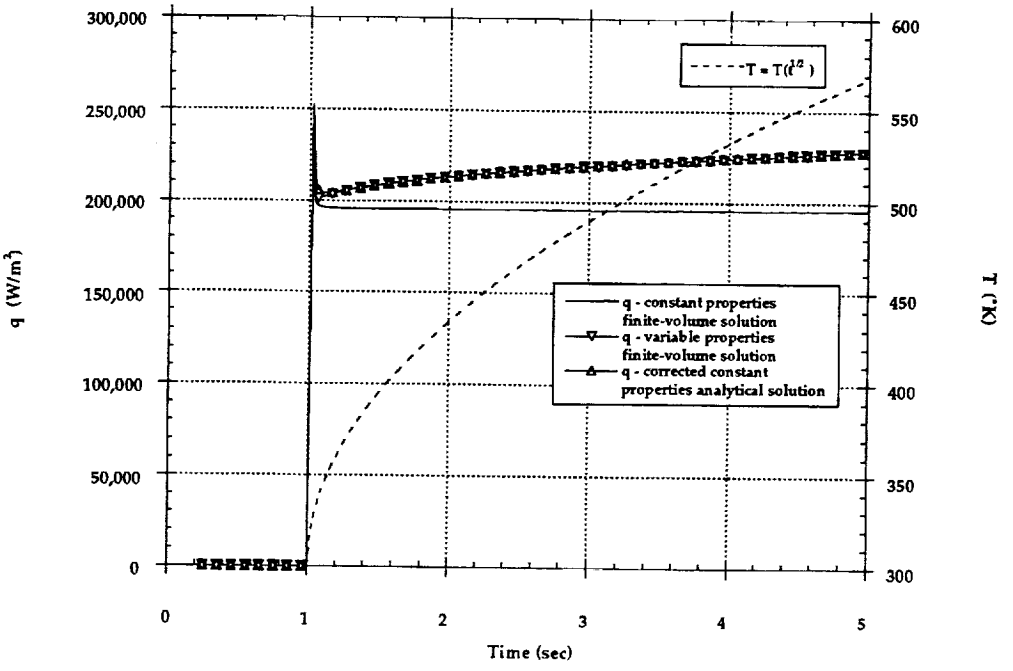


FIGURE 31: Finite-volume solution and corrected analytical solution for stagnation point thin-film gage

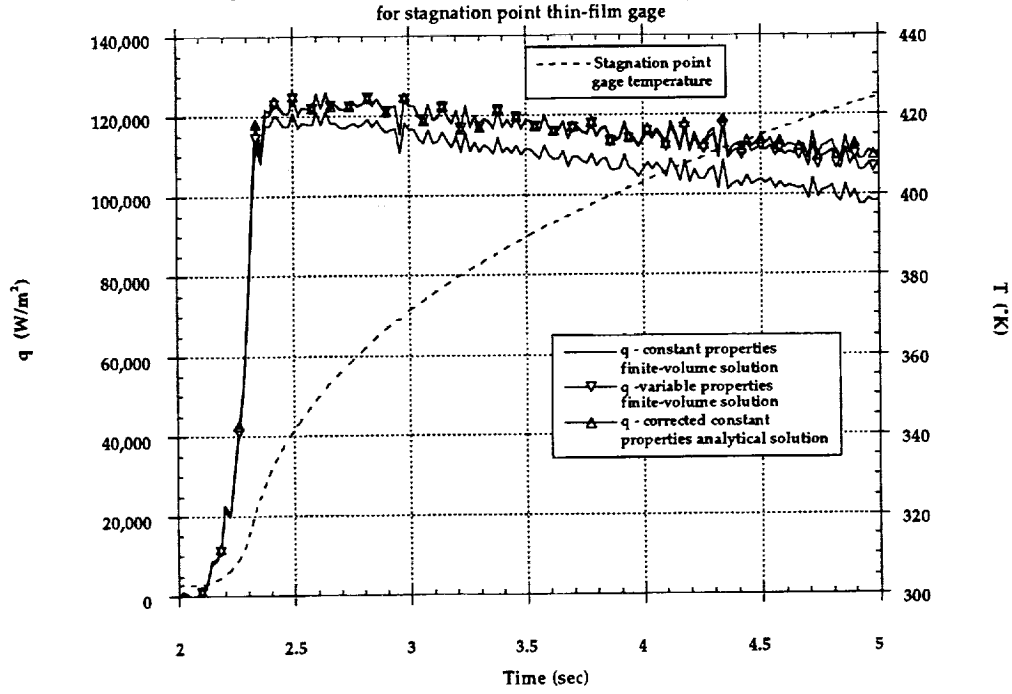
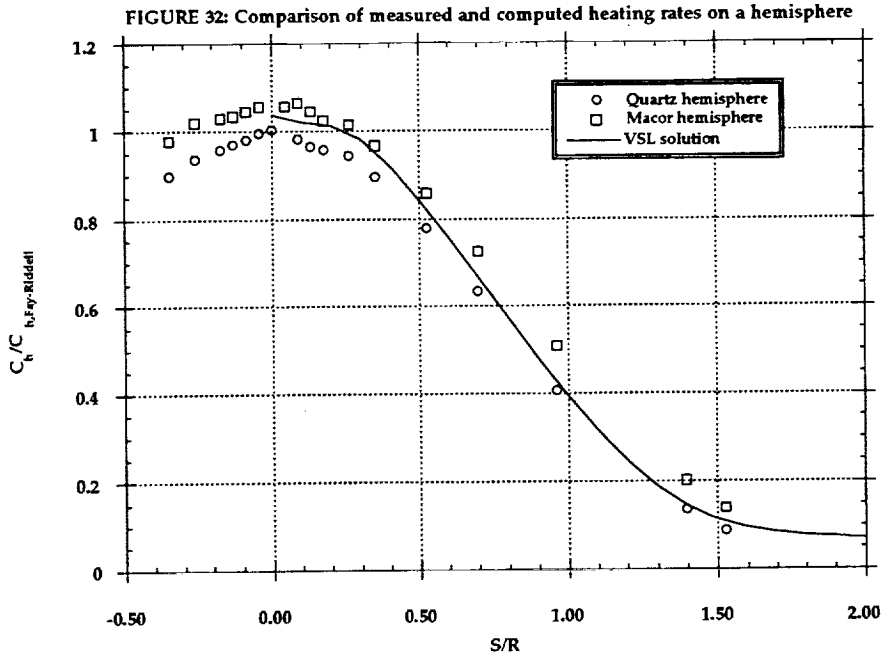


FIGURE 32: Comparison of measured and computed heating rates on a hemisphere



REPORT DOCUMENTATION PAGE

Form Approved
OMB No. 0704-0188

Public reporting burden for this collection of information is estimated to average 1 hour per response, including the time for reviewing instructions, searching existing data sources, gathering and maintaining the data needed, and completing and reviewing the collection of information. Send comments regarding this burden estimate or any other aspect of this collection of information, including suggestions for reducing this burden, to Washington Headquarters Services, Directorate for Information Operations and Reports, 1215 Jefferson Davis Highway, Suite 1204, Arlington, VA 22202-4302, and to the Office of Management and Budget, Paperwork Reduction Project (0704-0188), Washington, DC 20503.

1. AGENCY USE ONLY (*Leave blank*)	2. REPORT DATE	3. REPORT TYPE AND DATES COVERED
	August 1995	Contractor Report

4. TITLE AND SUBTITLE
User's Manual for the One-Dimensional Hypersonic Experimental Aero-Thermodynamic (1DHEAT) Data Reduction Code

5. FUNDING NUMBERS
G NAG1-1663 and NASW-1331

WU 242-20-08-02

6. AUTHOR(S)
Brian R. Hollis

7. PERFORMING ORGANIZATION NAME(S) AND ADDRESS(ES)
North Carolina State University
Dept. of Mechanical and Aerospace Engineering
Raleigh, NC 27695

8. PERFORMING ORGANIZATION REPORT NUMBER

9. SPONSORING / MONITORING AGENCY NAME(S) AND ADDRESS(ES)
National Aeronautics and Space Administration
Langley Research Center
Hampton, VA 23681-0001

10. SPONSORING / MONITORING AGENCY REPORT NUMBER
NASA CR-4691

11. SUPPLEMENTARY NOTES
Langley Technical Monitor: Harris H. Hamilton II

12a. DISTRIBUTION / AVAILABILITY STATEMENT
Unclassified -- Unlimited
Subject Categories 34, 61, and 35

12b. DISTRIBUTION CODE

13. ABSTRACT (*Maximum 200 words*)

A FORTRAN computer code for the reduction and analysis of experimental heat transfer data has been developed. This code can be utilized to determine heat transfer rates from surface temperature measurements made using either thin-film resistance gages or coaxial surface thermocouples. Both an analytical and a numerical finite-volume heat transfer model are implemented in this code. The analytical solution is based on a one-dimensional, semi-infinite wall thickness model with the approximation of constant substrate thermal properties, which is empirically corrected for the effects of variable thermal properties. The finite-volume solution is based on a one-dimensional, implicit discretization. The finite-volume model directly incorporates the effects of variable substrate thermal properties and does not require the semi-finite wall thickness approximation used in the analytical model. This model also includes the option of a multiple-layer substrate. Fast, accurate results can be obtained using either method. This code has been used to reduce several sets of aerodynamic heating data, of which samples are included in this report.

14. SUBJECT TERMS
Heat Transfer
Thin-Film Resistance Gage
Coaxial Surface Thermocouple

15. NUMBER OF PAGES
72

16. PRICE CODE
A04

17. SECURITY CLASSIFICATION OF REPORT	18. SECURITY CLASSIFICATION OF THIS PAGE	19. SECURITY CLASSIFICATION OF ABSTRACT	20. LIMITATION OF ABSTRACT
Unclassified	Unclassified	Unclassified	